

OPTICAL AND NEAR-INFRARED *UBVRIJK* PHOTOMETRY FOR THE RR LYRAE STARS IN THE NEARBY GLOBULAR CLUSTER M4 (NGC 6121)*

P. B. STETSON¹, V. F. BRAGA², M. DALL'ORA³, G. BONO^{2,4}, R. BUONANNO^{2,5}, I. FERRARO⁴, G. IANNICOLA⁴, M. MARENGO⁶, J. NEELEY⁶

(Dated: Submitted August 31, 2021 / Received / Accepted)
Draft version August 31, 2021

ABSTRACT

We present optical and near-infrared *UBVRIJK* photometry of stars in the Galactic globular cluster M4 (NGC 6121) based upon a large corpus of observations obtained mainly from public astronomical archives. We concentrate on the RR Lyrae variable stars in the cluster, and make a particular effort to accurately reidentify the previously discovered variables. We have also discovered two new probable RR Lyrae variables in the M4 field: one of them by its position on the sky and its photometric properties is a probable member of the cluster, and the second is a probable background (bulge?) object. We provide accurate equatorial coordinates for all 47 stars identified as RR Lyraes, new photometric measurements for 46 of them, and new period estimates for 45. We have also derived accurate positions and mean photometry for 34 more stars previously identified as variable stars of other types, and for an additional five non-RR Lyrae variable stars identified for the first time here. We present optical and near-infrared color-magnitude diagrams for the cluster and show the locations of the variable stars in them. We present the Bailey (period-amplitude) diagrams and the period-frequency histogram for the RR Lyrae stars in M4 and compare them to the corresponding diagrams for M5 (NGC 5904). We conclude that the RR Lyrae populations in the two clusters are quite similar in all the relevant properties that we have considered. The mean periods, pulsation-mode ratios, and Bailey diagrams of these two clusters show support for the recently proposed “Oosterhoff-neutral” classification.

Subject headings: Stars; Star Clusters and Associations

1. INTRODUCTION

The Galactic globular clusters (GGCs) NGC 6397 and M4 (NGC 6121) play a key role among all the GGCs, since these are the closest two globulars to the Sun. Unlike NGC 6397, M4 is located near the equator ($\alpha = 16^{\text{h}} 23^{\text{m}} 35^{\text{s}}$, $\delta = -26^{\circ} 31' 32''$), making it a good target for both northern and southern observing facilities. Again unlike NGC 6397, M4 hosts a significant population of RR Lyrae variables, which offers a whole new class of observational constraints on the cluster's distance and physical properties. The main drawback of M4 is that it is veiled by large and differential reddening: $E(B-V) = 0.37 \pm 0.01$ (estimated standard error of the mean, overall range $\delta E(B-V) \gtrsim 0.2$ mag) according to Hendricks et al. (2012) (hereinafter

H12); see also Ivans et al. (1999), Marino et al. (2008) and Mucciarelli et al. (2011). Furthermore, several studies in recent years have suggested that the reddening law toward M4 is abnormal compared to the canonical diffuse interstellar medium (Cardelli, Clayton & Mathis 1989; McCall 2004). These drawbacks are due to the fact that M4 is located behind the Scorpius-Ophiuchus cloud complex. The problem of the reddening law in the direction of M4 has been recently discussed in a thorough investigation by H12 on the basis of both optical and near-infrared (NIR) photometry.

Its small distance makes M4 a valuable laboratory for stellar evolution studies, since even modest telescopes can provide accurate photometric and spectroscopic data well below the main-sequence turnoff. The same consideration applies to variable stars, and indeed M4 hosts a sizable sample of stars identified as fundamental (FU, 31) and first overtone (FO, 13) RR Lyraes (Clement et al. 2001), and optical photoelectric photometry has been published for a significant fraction of them (Sturch 1977; Cacciari 1979; Liu & Janes 1990; Clementini et al. 1994). A sizable sample of eclipsing binaries has been detected and studied by Kaluzny et al. (1997), Mochejska et al. (2002), Kaluzny et al. (2013a) and Kaluzny et al. (2013b). A detailed X-ray and optical investigation of the innermost cluster regions was performed by Bassa et al. (2004), who detected a dozen chromospherically active binaries, confirmed the presence of a millisecond pulsar (Lyne et al. 1988; Sigurdsson et al. 2003), and identified a couple of candidate cataclysmic variables. More recently, deep optical imaging with the Advanced Camera for Surveys (ACS) on the *Hubble Space Telescope* (HST) has provided a very deep color-magnitude diagram approaching the hydrogen burning limit on the main sequence, and showing the blue hook on the white dwarf cooling sequence (Hansen et al. 2004).

A deep and accurate optical–NIR CMD based on images

* Based in part on data obtained from the ESO Science Archive Facility under multiple requests by the authors; in part on data obtained from the Isaac Newton Group Archive, which is maintained as part of the CASU Astronomical Data Centre at the Institute of Astronomy, Cambridge; and in part upon data distributed by the NAO Science Archive. NAO is operated by the Association of Universities for Research in Astronomy (AURA) under cooperative agreement with the National Science Foundation. This research also benefited from the Digitized Sky Survey service provided by the Canadian Astronomy Data Centre operated by the National Research Council of Canada with the support of the Canadian Space Agency.

¹ NRC-Herzberg, Dominion Astrophysical Observatory, 5071 West Saanich Road, Victoria BC V9E 2E7, Canada

² Department of Physics, Università di Roma Tor Vergata, via della Ricerca Scientifica 1, 00133 Roma, Italy

³ INAF-Osservatorio Astronomico di Capodimonte, Salita Moiariele 16, 80131 Napoli, Italy

⁴ INAF-Osservatorio Astronomico di Roma, via Frascati 33, 00040 Monte Porzio Catone, Italy

⁵ INAF-Osservatorio Astronomico di Teramo, Via Mentore Maggini snc, Loc. Collurania, 64100 Teramo, Italy

⁶ Department of Physics and Astronomy, Iowa State University, Ames, IA 50011, USA

collected with HST was provided by Milone et al. (2014). They found evidence of a split in the main sequence region located below the knee. In particular, they found that one subpopulation can be associated with normal chemical abundance ratios, and the other with a composition that is enhanced in nitrogen and depleted in oxygen.

This result appears even more compelling in conjunction with the results of a very detailed spectroscopic analysis of evolved and main-sequence stars performed by Malavolta et al. (2014). They collected a large number of high-resolution spectra for more than two thousand cluster members and found that the overall metallicity is almost constant over the entire sample: $[Fe/H] = -1.07$, $\sigma = 0.02$. Moreover, the difference in iron content between the two distinct stellar sequences along the RGB of M4, identified by Monelli et al. (2013), is smaller than 0.01 dex. This is consistent with the evidence from Milone et al. (2014) that the difference appears to be in the CNO abundances.

A deep and accurate NIR CMD of M4 was also provided by Libralato et al. (2014), who analysed NIR images collected with HAWK-I at VLT. Their data cover a time interval of eight years, and accurate ground-based astrometry allowed them to distinguish cluster and field stars.

This is a paper in a series dedicated to multiband photometry of cluster and field RR Lyrae stars. In §§2 and 3 below, we present both optical and NIR data sets for the variable stars of M4. Then §4 deals with the reidentification and characterization of the variable stars in the cluster field, while §5 considers them in the context of the cluster color-magnitude diagram. After that, §6 discusses the pulsation properties of the RR Lyrae variables and the implications for their evolutionary status, and §7 compares and contrasts the RR Lyrae population of M4 to that of another well-studied cluster, M5 (NGC 5904). Finally, §8 briefly summarizes the results of our study.

2. OPTICAL PHOTOMETRY

Our optical observations of M4 consist of 5,003 individual CCD images obtained during the course of 18 observing runs. Table 1 is a synopsis of the observation dates and the number of exposures obtained in each filter during each run. The column “multiplex” refers to the number of individual CCD chips in the particular camera, which were treated as independent detectors. The multiplex factor times the number of exposures represents the net contribution to the grand total of 5,003 CCD images cited above.

These observations were included in a total of 84 datasets, where a dataset is defined as either (a) all the digital images obtained with a single CCD chip on a single photometric night, or (b) all the digital images obtained with a single CCD on one or more non-photometric nights during the same observing run. Datasets from photometric nights are calibrated with respect to standard stars in many fields spread across the sky, including full corrections for atmospheric extinction. Datasets from non-photometric nights are calibrated with respect to local standards contained within each image, which have themselves been established on photometric occasions. (Datasets from nights when science targets *only* were observed, with no fundamental photometric standard-field observations, were also treated as non-photometric.) Color-transformation coefficients can be derived for non-photometric datasets just as for photometric ones, provided that stars of a range of color are available in at least some individual images; this was always the case here. Of the 84

datasets containing our observations of M4, 37 were considered to be of photometric quality, and the remaining 47 were treated as non-photometric.

All the CCD images were reduced by PBS using the DAOPHOT/ALLSTAR/ALLFRAME suite of programs. These data were then calibrated to the Johnson *UBV*, Kron/Cousins *RI* photometric system of Stetson (2000, 2005)⁸, which is designed to be as close as possible to that of Landolt (1992); see also Landolt (1973, 1983). The photometric standard values that were employed here were those current as of 2013 August 13. By comparison with Landolt’s published values for stars in common, we determine that this photometric system agrees with Landolt’s with an rms dispersion *per star* of 0.028 mag in *U*, 0.018 mag in *B*, 0.013 mag in *V*, 0.011 mag in *R*, and 0.015 mag in *I*, based upon 203, 325, 339, 216, and 230 individual stars common to the two samples, respectively. We believe that these numbers represent a fundamental limit to the accuracy with which these broad-band photometric indices for any given star can be transformed from one filter set to another, given the variety present among stellar spectral-energy distributions. *In the mean*, our system appears to agree with Landolt’s to $\lesssim 0.001$ mag (68% confidence interval) in *BVRI* and to $\lesssim 0.002$ mag in *U* for stars in the magnitude range of overlap ($7.6 \leq V \leq 16.1$). The equivalence of the two photometric systems at fainter magnitudes relies primarily on the reliability of the shutter timings in the various cameras used for our observations; we fully expect these to be accurate to well under 1%.

For service as a local standard in the M4 field, suitable for use in the final transformation of all instrumental magnitudes to the adopted standard photometric system, we identified by eye stars that appeared to be relatively free from blending with neighboring stars. We further required that each star have been observed in a given filter on at least three photometric occasions, have a derived standard error of the mean magnitude in that filter ≤ 0.04 mag, and have no evidence of intrinsic variability in excess of 0.05 mag, root-mean-square, based upon the repeatability of the available observations in all filters. These conditions were satisfied by 634, 875, 878, 308, and 877 stars in *U*, *B*, *V*, *R*, and *I*, respectively. (For comparison, our usual stricter selection criteria—specifically, at least *five* independent observations on photometric occasions and standard errors < 0.02 mag in at least *two* filters, as well as repeatability better than 0.05 mag, r.m.s.—were satisfied by 251, 856, 860, 298, and 857 of these stars, respectively.) These stars were then used as a local reference for the photometric calibration of all optical measurements of stars in M4 from the final ALLFRAME reduction. This analysis resulted in 64,626 stars in the M4 field with calibrated photometry in *V* and at least one of *B* or *I*; 62,943 stars had calibrated photometry in all three of *B*, *V*, and *I*; and 18,218 of them had calibrated photometry in all five of *U*, *B*, *V*, *R*, and *I*.

Since any given CCD image spans only a fraction of the total field covered by all our observations, no star appears in every image. In fact, the *maximum* number of calibrated magnitude measurements for any given star was 12 in *U*; 1,110 in *B*; 1,510 in *V*; 1,817 in *R*; and 42 in *I*. Considering only stars with at least one observation in a given filter, the median number of observations was 4 in *U*, 21 in *B*, 31 in *V*, 1770 in *R*, and 14 in *I*. Since most observations were centered near the cluster, member stars preferentially have more than the

⁸ <http://www1.cadc-ccda.hia-ihp.nrc-cnrc.gc.ca/community/STETSON/standards/>, see also <http://www.cadc.hia-ihp.nrc.gc.ca/community/STETSON/homogeneous/archive/>

median number of observations; stars in the outer part of the field where smaller numbers of observations had been made were more likely to be field stars. Indeed, for the stars that we considered to be variable candidates in the study below, the median number of observations was 9 in *U*, 1,106 in *B*, 1,495 in *V*, 1,813 in *R*, and 30 in *I*.

An additional 36,207 stars were included in the ALLFRAME reductions, but they fell outside the area where adequate observations exist to define local photometric standards; for these stars, astrometric information is available, but no calibrated photometry is possible at present.

3. NEAR INFRARED PHOTOMETRY

The infrared photometry for M4 consisted of 55 datasets from 18 observing runs, as outlined in Table 2. As with the optical data, all photometric measurements were carried out by PBS using the DAOPHOT/ALLSTAR/ALLFRAME suite of programs. Calibration of the data was slightly different from the optical case, in that we are able to use the point-source catalog of the Two Micron All Sky Survey (2MASS)⁹, which provides calibrated *JHK* photometry for stars in virtually all our images. This gives us the option of applying the “non-photometric” calibration approach described in the previous section to obtain fundamentally calibrated magnitudes on a well-defined system, without the need to consider extinction corrections among observations obtained at various airmasses.

For our purposes we selected only those published 2MASS magnitudes that were flagged as of photometric quality “A,” implying an estimated standard error of the adopted magnitude $\sigma \leq 0.1086$. A total of 11,919 2MASS stars having a quality “A” magnitude in at least one of the three filters could be identified with entries in our own catalog of stars in the target field within a one-arcsecond match-up tolerance, after modest astrometric transformations had reduced the r.m.s. astrometric differences from $0''.28$ in the RA direction and $0''.21$ in the Dec direction to $0''.19$ in each coordinate.

With these stars initially adopted as photometric standards, robust fitting techniques (see Stetson 1989) were used to estimate photometric transformations from the instrumental system of each of our infrared datasets to the photometric system of the 2MASS catalog. The transformations involved linear color transformations, photometric zero points, and linear zero-point gradients in *x* and *y* across the face of each detector:

$$j(\text{observed}) = J(\text{standard}) + z + ax + by + c(J-K)$$

etc. Average values of *a*, *b*, *c* were computed for each detector chip and each observing run, and a separate value of *z* was obtained for each digital image.

There were two exceptions to this approach. First, run 1 (designated “m4ir” in Table 2) seemed to be of such good quality that we adopted the full photometric-night reduction scheme, including explicit extinction corrections and field-to-field photometric tie-in. This helped to ensure a uniform photometric calibration among the different images, which were individually rather small and contained relatively few 2MASS stars apiece. Second, the images obtained with MAD—the multi-conjugate adaptive-optics demonstrator on the VLT

(Marchetti et al. 2006)—were so deep, so small, and so close to the cluster center that they contained no unsaturated images of high-quality 2MASS stars. In order to calibrate these data, we used our measurements of fainter stars contained within the other datasets, calibrated to the 2MASS system, to serve as local secondary standards for the MAD data.

After an initial calibration was found for all of the datasets excepting “mad3,” the transformations were applied to our instrumental magnitudes for the 2MASS standards, weighted averages were taken, and the results compared to the 2MASS magnitudes for the same stars. Those showing the largest residuals were rejected from consideration as local standards, and new photometric transformations were derived from all the datasets employing the more restricted set of local 2MASS standards. This was repeated until all stars showing residuals larger than 0.30 mag in any of the three filters had been eliminated. At the end, our photometric calibration relies on a total of 7,901 2MASS stars with valid measurements in *J*; 5,847 in *H*; and 3,389 in *K*. Computed values of the zero-point gradients (*a*, *b*) ranged between extreme values of -0.151 and $+0.048$ mag per 1000 pixels, and the standard deviation among all the chips and runs was about 0.015 mag per 1000 pixels. The local 2MASS standards permitted us to measure these gradients with a typical precision of 0.002 mag per 1000 pixels. The color-transformation coefficients *c* took on values ranging from -0.122 to $+0.225$, depending upon filter and camera, with a standard deviation among the chips/runs of about 0.16; the 2MASS stars determined these coefficients with a typical precision of 0.008 mag/mag. The median precision for the adopted zero-point, *z*, of an individual exposure was 0.008 mag.

The root-mean-square residual between the published 2MASS magnitudes and our averaged calibrated photometry for the same stars is measured to be 0.063, 0.064, and 0.069 mag per star in *J*, *H*, and *K*. We take these as upper limits for the statistical reliability of our average magnitude for any given star in any given filter, since uncertainties in the 2MASS magnitudes as well as our own contribute to the observed scatter, and the 2MASS sample includes stars whose 2MASS standard errors are estimated to be as large as 0.11 mag. Dividing these r.m.s. residuals by the square root of *N* suggests that the formal standard error in transforming our instrumental magnitudes to the 2MASS system should be ~ 0.001 in the mean, but surely this is unrealistic: unknown systematics could be considerably larger than this. For instance, we are not in a position to judge whether there may be zone errors in the 2MASS Point Source Catalog, such that this particular patch of sky including the globular cluster M4 may be on a slightly different photometric system than other parts of the sky in the same catalog.

As mentioned above, the MAD data were calibrated using a secondary set of local standards that we ourselves have selected and referred to the 2MASS system. We defined 90 of these local standards, and there were a total of 11,844 individual magnitude measurements for these 90 stars among the 152 MAD images. These had observed standard errors of 0.073 mag per measurement, or 0.021 mag, r.m.s., per star, between the average of the MAD magnitudes and the average of our magnitudes for the same stars from the other runs.

4. VARIABLE STARS

4.1. Identification

⁹ The 2MASS Point Source Catalog was produced by a joint project of the University of Massachusetts and the Infrared Processing and Analysis Center, funded by the National Aeronautics and Space Administration and the National Science Foundation.

Our optical photometry has several advantages when compared with the various sets of time-series data available in the literature. (a) In the present case, the number of consecutive observations on any given single night could be as large as 125 in any one filter, and up to 270 observations in all filters. This means that we have, for a significant fraction of objects, a number of measurements in some filters on consecutive nights that ranges from several tens to several hundred. (b) The photometric data span a large time interval (16 years). This allows for very accurate period determinations and the opportunity to identify variables with periods close to 0.5 days. (c) The phase coverage is quite good in at least three photometric bands, namely B , V and R . This also means that we can use three different colors and brightness amplitudes to constrain the stars' pulsation properties (see §5). (d) Our photometry of at least some of the known RR Lyrae variables can be supplemented with photoelectric photometry available in the literature (Sturch 1977; Cacciari 1979; Liu & Janes 1990; Clementini et al. 1994). This will allow us to further constrain their pulsation properties (Blazhko effect, amplitude modulation), and gives us a chance, at least, to look for evolutionary effects (period changes).

We carried out independent identification of candidate variable stars using the Welch & Stetson index (WS, Welch & Stetson (1993); Stetson (1996)) as applied to our optical data set. In particular, we considered all stars with a weight (defined as the number of consecutive image pairs, plus one-half the number of unpaired singleton images in which the star appears) greater than $w = 180$. We designated as candidates stars having a WS index larger than 0.8; 242 stars met this criterion, representing 0.9% of all stars with $w \geq 180$. A number of the variable stars listed in Clement's catalog failed to meet these criteria: V43 had no data at all, falling outside the field spanned by our images; stars V3, V29, V32, V33, V34, V42, V75, V76, and V79 had insufficient weight, falling in the less-well-observed outer parts of the cluster; and V17, V44, V45, V46, V47, V48, V50, V51, V53, V54, V55, V56, V57, V58, V59, V60, V65, V71, V78 and V80 had WS indices < 0.8 . We added these stars to the list of candidate variables by hand, so that our software would extract their light-curve data. We will discuss these stars individually now.

4.2. Comparison with Clement's catalog

Christine Clement's on-line catalog ("Updated 2009s") lists 79 stars in M4 identified as variable (they are numbered V1 through V80, but V62 is identified as equal to V55). Of these 79 stars, 67 are listed with equatorial coordinates having a precision of $1''$ or better; nine have (x, y) coordinates with a precision of $0''.1$; and three have references to finding charts only, with no positions given.

For the 67 Clement stars with equatorial coordinates, we transformed her positions to (x, y) in our coordinate system, and cross-matched with our photometric catalog for M4 without regard to whether our stars appeared variable. With simple translations in x and y , we were able to match 66 of the 67 stars within a tolerance of $2''$, with offsets of $-0''.2$ and $-0''.5$ in x and y , and a star-to-star dispersion of $0''.5$ in each coordinate. Four-constant and six-constant linear transformations did not improve the agreement. The star that could not be matched to any star in our photometry catalog was Clement's V43; her published position for this star falls outside the area covered by our images. Of the 66 matching stars, 58 of the matches were unique: no other star in our catalog was present

within $2''$ of Clement's positions (as transformed to our reference frame).

In each of the other eight cases, there were two stars in our catalog within $2''$ of the Clement position: V21, V40, V65, V69, V70, V72, V73, and V78. Among these, V21 was not ambiguous: the star closer to the predicted position had the right apparent magnitude and color to be an RR Lyrae and had strong evidence of variability in our data; the other star was 2.8 mag fainter and showed no evidence of intrinsic variation. In the case of V40, both matches had roughly suitable magnitudes and colors, and both showed strong evidence of variability; we retain both stars, identifying the closer and brighter match with Clement's V40 and designating the fainter and more distant one new variable candidate C1. Among the other six cases, there were only two where one star of the pair showed evidence of variability. For V69 (this star is also identified as K50), a $V = 17.3$ star $1''.9$ from the predicted position showed strong evidence of variability while a $V = 16.7$ star $0''.4$ from the predicted position did not. In the case of V73 (this star is also identified as K54), a $V = 17.8$ star $1''.8$ from the predicted position showed mild evidence of variability while a $V = 19.9$ star $0''.6$ from the position did not. For these two cases, we have provisionally identified Clement's star with the one in our data that showed evidence of variation despite the fact that it was farther from the predicted position than the alternative.

In the final four cases (V65, V70, V72, and V78), neither star appeared to be variable in our data. However, for V65, V70, and V78 we were able to make an unambiguous match by comparing our measured mean magnitudes for these stars to those given in Clement's table. V72 is the lone remaining star. Clement gives $B_{\max} = 16.34$ for this star, with an amplitude in B of 0.3 mag. Our two stars within $2''$ of the predicted position have $\langle B \rangle = 19.17$ and 18.42. But $2''.01$ from the predicted position there does lie a star with $\langle B \rangle = 16.46$ and strong evidence of variability. Accordingly we adopt this star as the match. Alerted by this, we checked the apparent magnitudes of the other, seemingly unambiguous matches, and found that V67 (= K48), V68 (= K49), V71 (= K52), and V73 (= K54) had probably been misidentified; in each case another star more than $2''.0$ but less than $2''.5$ from the predicted position appeared to be a better photometric match, and accordingly these changes were made.

The star V17 turned out to be a special case. Clement gives equatorial coordinates for this star, and there was exactly one star in our sample within $2''.0$ of this position; in fact, after the modest astrometric transformation that we have applied, our star is $0''.31$ from the position recorded by Clement. However, Clement gives the mean B -band magnitude of V17 as 13.55, while our star has $B = 14.19$ and a $B-V$ color of 1.30, which is much too red for an RR Lyrae. Furthermore, Clement says that the period of this star is 0.8555 days—which is unusually long for an RR Lyrae—while our star shows no evidence of variability. However, we note that at the reported position of Clement's star V52 we do find an RR Lyrae with a period of 0.8555 days (§4.3 below). According to Clement, V17 has equatorial coordinates $16^{\text{h}}23^{\text{m}}34^{\text{s}}.02 - 26^{\circ}31'07''.8$ while she gives the position of V52 as $16^{\text{h}}23^{\text{m}}24^{\text{s}}.08 - 26^{\circ}30'27''.6$, suggesting that at some point a transcription error changed the right ascension of V52 by 10 seconds of time, possibly creating a fictitious V17. We further note that according to Clement the coordinates of variable V18 are $16^{\text{h}}23^{\text{m}}34^{\text{s}}.69 - 26^{\circ}31'03''.9$, which might possibly account for the recorded

declination of V17 assuming that someone made a slip of one line in reading a table. This attempted reconstruction of history is purely conjectural. All that we can state with certainty is (a) at Clement’s recorded position for V17—which she attributes to a 2009 private communication from Samus—we find no RR Lyrae at all, let alone an RR Lyrae with the unusual period of 0.8555 d; (b) at Clement’s recorded position for V52 there is an RR Lyrae with the period of 0.8555 d (she lists 0.4605 d as the period of V52, while we find *no* RR Lyrae in M4 with a period between 0.455 and 0.463 d). For our purposes here, we drop Clement’s V17 from the list of candidate variable stars in M4 and retain the designation V52, but we revise the star’s period from 0.4605 to 0.8555 d.

The nine stars V53 through V61 have only (x, y) positions (referred to the nominal cluster center) in the Clement catalog. These are all supposed to be fairly luminous stars, so it was easy to plot their predicted positions on our stacked image of the cluster field and identify the closest bright star to each position. Quantitatively, the match required position offsets of $1''.7$ in each coordinate; the nine stars then matched nine bright stars in our catalog with a root-mean-square dispersion $< 0''.1$.

There are three variable candidates in Clement’s list with no positions given.

According to Clement, V75 is identified as star G343 in a finding chart published in (according to Clement) Greenstein (1939 ApJ 90, 401) but the correct citation appears to be Greenstein (1939 ApJ 90, 387; Greenstein (1939)); the relevant chart itself appears as Plate V in that paper. We have identified this star in our image of the field. The star does not show strong evidence of variation in our data, but the number of our observations is comparatively small.

V79 is also supposed to appear in Greenstein’s chart as star G302. A dot representing that star is not actually visible either in the on-line reproductions of Greenstein’s chart, or in the photographic reproduction of his plate in the paper copy of the journal. However, in our digital image of the field, there is a blended pair of stars between stars G299 and G303, at a position where it would lie just to the left of the label “302” in Greenstein’s plate. Of these two, the southeastern star has strong evidence of intrinsic variability in our data; we identify this as V79.

According to Clement, V76 is equal to star ZB14, identified by (x, y) position and finding chart in (Yao 1977). We have examined this paper to the extent possible, given that none of us can read Chinese. We find equatorial coordinates and finding charts for two stars, ZB12 and ZB13, but nothing that appears to be a position for ZB14. There is a plate in the paper, Plate 2, whose caption does not mention ZB14 in characters that we are able to read, but there is only one star marked in this plate. We have identified this same star in our data, and find that it has quite strong evidence of intrinsic variability on a timescale appropriate for an RR Lyrae variable, although the number of our measurements of this star is comparatively small. Furthermore, the measurements that we do have for this star imply a magnitude and colors appropriate for an RR Lyrae at the cluster distance. On the working hypothesis that this is Yao’s star ZB14, we provisionally identify it as V76. We remind the reader that we have no direct evidence that Plate 2 in the Yao paper is intended to be a finding chart for ZB14; this is purely conjecture on our part.

Among the other stars that we identified in our catalog with $WS > 0.8$ and $wt \geq 180$ most could be attributed to bad data of one sort or another. There was one other star, however, whose

magnitudes could be phased into a good RR Lyrae light curve. We designate this star C2. Fig. 1 shows the optical-band light curves for the newly identified RR Lyrae candidates C1 and C2.

We list our equatorial positions for the stars we have identified as RR Lyrae variables in the M4 field in Table 3, while Tables 4 and 5 give photometric parameters in, respectively, the optical and near-infrared bands for the RR Lyrae stars. “V” star names are the identifications assigned by Clement; as already mentioned, we have assigned “C” names to the new candidate variables identified here for the first time. For the convenience of the reader, in Tables 4 and 5 we also provide “K” designations from the studies of Kaluzny et al. (1997, 2013a and 2013b).

We include V76 in these tables because in our limited data for the star, we see short-term (i.e., over the course of an hour or so) increases and decreases in brightness, parallel in B and V , and consistent with the rates expected for an RR Lyrae. However, our data are not extensive enough to obtain a period.

As already mentioned, Clement’s catalog also identifies a number of candidate variable stars that are apparently not of the RR Lyrae type. Table 6 gives our recovered positions, average optical photometry, and a comment for each of these, while Table 7 gives average NIR photometry for the same variable candidates. In addition, we have looked for ten more variable candidates from Kaluzny et al. (2013b) that were not included in Clement’s compilation, K58–66 and K68, and one more from Kaluzny et al. (2013a), K69. We used their tabulated coordinates for these stars to establish their approximate locations on our stacked image of the field, and then compared our image to their postage-stamp finding charts to confirm that the correct stars had been identified. We were unable to recover their star K58; if their tables and chart are correct, then K58 is a $V \approx 20.4$ object closely blended with a $V = 16.38$ star in our data, and we did not distinguish it as a separate object. Finally, we include five more new candidate variables that we have identified for the first time here (C3–C7).

Among these stars, V53 shows some evidence for variability on timescales of minutes to hours, but we are not able to come up with a phased light curve or period. Stars V54–V60 and also V65 (= K46) and K63 have been called “LPV or EB?” because our data show some (in some cases slight) evidence of different mean magnitudes in at least one of B , V , or R from different observing runs, but no evidence of coherent variation *within* any single observing run. Conversely, of course, it is possible that some of these stars are subject to crowding or other photometric defects. We would not have dared to identify any of them as variable candidates on the strength of our own data, had they not already been so designated in the literature. V77 (= K56) is mostly constant in brightness, but on Julian day 2451702 it does show one decrease and increase of about 0.06 mag in the B bandpass that looks very much like the bottom of an eclipse. For V78 (= K57) we have computed nightly average magnitudes in B , V , and R ; there is one night where it is 0.04 mag fainter in B than average of the 45 other nights when the star was observed in the B filter, and one night where it is 0.08 mag fainter in V than the average of the 44 other nights when V was observed, but they are not the same night, nor are they from the same run. There is no other evidence than this in our data that the star we have identified as V78 is variable. We also have fairly extensive data for V80, and do not see evidence for variability on time scales of either hours, days, or years. The other candidates, for all of which we list periods in Table 6, are al-

most certainly eclipsing binaries except perhaps C3. We are not sure of its classification, but with a sinusoidal light curve, small amplitude, and a provisional period of 19 days (and it is possible that this is an alias of the true period) it could perhaps be a background semiregular variable. In Figs. 2 and 3 we illustrate the light curves of the new variables C3–C7.

In Fig. 4 we show the positions of all the non-RR Lyrae variable candidates in the color-magnitude diagram of M4. For this diagram, we adopt $B-I$ as the color because several of the candidates are missing R -band magnitudes, but all have I . Note that two of our newly discovered candidates (C6 at $V, B-I = 18, 2.4$ and C7 at $19, 2.9$) lie on M4's binary main sequence; they are thus good candidates for cluster membership. These stars will not be discussed further in this paper.

4.3. Characterization of the variability

A period search was performed for all candidates using a robust string-length algorithm that we have developed (Stetson 1996; Stetson et al. 1998). This identifies the best candidate period from simultaneous consideration of the calibrated measurements and their associated standard errors in all available photometric bands. (In our case, we used $BVRI$; U was omitted because of the comparatively small number and relatively poor quality of measurements. It must be pointed out that the I -band data contributed relatively little weight to this procedure.) The graphical display incorporated in our software makes it easy to distinguish real periodic variability from corrupt data, and the stars displaying the latter rather than the former were manually triaged out of our sample at this point. The type of variability (e.g., fundamental-mode RR Lyrae, first overtone RR Lyrae, Blazhko effect; eclipsing binary; long-period variable) is also fairly evident at this point and we were able to enter this information in our notes. Once the best candidate period had been identified, Fourier series were then fitted by nonlinear least-squares to refine the candidate periods and estimate the mean magnitudes and amplitudes in the different photometric bands.

These initial estimates of the variables' properties were then independently confirmed or challenged by different co-authors employing two other algorithms:

(1) In our variant of the Lomb-Scargle method (Scargle 1982) algorithm, the candidate period is identified employing simultaneously all the measurements available in the different photometric bands ($UBVR$). A graphical interface allows fine tuning of the candidate period.

(2) Our new version of the PDM method (Stellingwerf 2011) identifies the period using only the measurements in the photometric band with the largest number of measurements and/or the largest time interval covered.

For this stage of the analysis, our own measurements of the M4 variable candidates were supplemented by whatever time-stamped observations were to be found in literature. All our initial classifications of the reality and type of variability were unchanged by this confirmation/challenge step. The difference in the periods measured by the above methods are typically smaller than one part per one hundred thousand. Once we had agreed upon the period, the individual measurements were phased and we performed a fit of the $UBVR$ light curves using splines under tension. Some researchers feel that this method may be more robust for objects that show either noisy data or amplitude modulation. These analytical fits allowed us to reliably estimate the mean magnitudes, the brightness amplitudes, and the epochs of maximum light.

The numbers of measurements available in the I band are

too limited to perform analytical fits with the above methods. Therefore, having adopted the I -band template light curves for RR Lyrae stars that have been provided by Layden (1998) together with our new estimates of period, V -band amplitude and epoch of maximum, we performed a least-squares fit to estimate the mean I -band magnitude and amplitude for each star. Template light curves for the RR Lyrae stars in the U band are not yet available. For this reason, we have provisionally estimated the mean U -band magnitudes of the RR Lyraes either from the unweighted mean of individual measurements (29 stars) or with a spline fit (18 stars); obviously, these mean U -band magnitudes should be regarded as suggestive only, and scientific use should be made of them only with extreme caution.

Table 4 gives for each star, from left to right, the identification, the period based on the LS method, the mean $UBVR$ band magnitudes based on spline fits, the mean I -band magnitude based on the template fit, and the epoch of maximum light. We also give the U -, B -, V -, R - (spline fit) and I -band (template fit) amplitudes. For completeness, we have included V34, V43 and V76 in these tables despite the fact that we do not have independent photometric data for V43, and we are unable to perform a proper independent light-curve analysis from our skimpy data for V34 and V76.

As discussed above, we have cross-correlated our list of candidate variable stars with the list of variable and candidate variable stars provided by Clement et al. (2001). We confirm variability for 44 of her 45 RR Lyrae candidates (excluding V43, for which we have no photometric data of our own, but including V34 and V76, for which we have enough data to see significant brightness changes, but not enough to fit a light curve) and provide updated estimates of their periods for 43 (excluding V34 and V76, but including V43, for which we use published data). Our sample also includes the two newly discovered highly probable RR Lyraes (C1 and C2). In total, if we include the published photometry for V43 and the published periods for V34 and V76, there are 45 cluster RR Lyraes and two field RR Lyraes (C2 and V64) with periods that we believe are reliable, and photometry that we believe is useful.

Fig. 5 shows the positions on the sky of both the cluster and field RR Lyraes. The red squares show the positions of fundamental-mode pulsators, while cyan squares are for first-overtone pulsators. The positions of the two candidate field RR Lyrae stars are additionally marked by enclosing circles. A stacked digital image of our field in M4 and a list of the pixel coordinates of all the variable candidates can be found at our web site¹⁰.

5. THE RR LYRAES IN THE COLOR-MAGNITUDE DIAGRAM

Fig. 6 shows the $V, B-R$ color-magnitude diagram (CMD) of M4. (We use $B-R$ here because most stars have much better measurements in R than in I .) Stars were selected according to the number of measurements (≥ 10), the photometric standard error ($\sigma_{BVR} \leq 0.02$ mag), and the radial distance ($1' \leq r \leq 7'$) from the center of the cluster (which we have estimated to be $16^{\text{h}}23^{\text{m}}35^{\text{s}}.21, -26^{\circ}31'34''.7$, with an estimated uncertainty $\sim 1''$ in each coordinate). Contamination by field stars is quite evident below the cluster main sequence for $B-R$ colors ranging from 1.3 to 2.5. The high number of individual measurements in BVR allows us to have good photometric precision over the entire magnitude range. Fig. 7 shows the K versus

¹⁰ <http://www.cadc-ccda.hia-ih.nrc-cnrc.gc.ca/community/STETSON/homogeneous>

J – K color-magnitude diagram for M4.

In both Fig. 6 and Fig. 7 the red and cyan symbols represent the positions of fundamental-mode (FU) and first-overtone (FO) RR Lyraes, respectively (see §6 below for a more detailed discussion concerning the identification of the pulsation mode); the two probable field stars have circles around them and lie far from M4’s horizontal branch. The candidate Blazhko stars are marked with black crosses. As expected, FOs in M4 have mean B – R colors that are systematically bluer than FUs (Bono et al. 1997b).

The two candidate field RR Lyrae stars (C2, V64) are found at $V \sim 16$ and $V \sim 20$ mag ($K \sim 13.7$ and 17.4). The latter, V64, is quite interesting since its apparent magnitude places it in the outskirts of the Galactic halo. Recent photometric catalogs—the ASAS Survey (Pojmanski 2002), the QUEST Survey (Vivas et al. 2004), the NSVS survey (Kinemuchi et al. 2006), the LONEOS Survey (Miceli et al. 2008), the Catalina Real-time Transient survey (Drake et al. 2009; Djorgovski et al. 2011), the SEKBO survey (Akhter et al. 2012), the LINEAR Survey (Palaversa et al. 2013), the GALEX Time Domain Survey (Gezari et al. 2013) in the ultraviolet, and the Carnegie RRL Program (Freedman et al. 2012) in the mid-infrared—have included only a very few RR Lyraes in these halo regions. C2 lies at Galactic coordinates $(l, b) = (351, +16)$, and it appears 2.7 mag fainter in V than the RR Lyraes in M4 ($\langle V \rangle = 16.04$ versus 13.32 —the median of the mean V magnitudes for 45 RR Lyraes in M4). Thus, all other things being equal, C2 is 3.5 times farther away than M4, or 7.7 kpc if we take 2.2 kpc as the distance to M4. This implies a Z -distance of 2.1 kpc above the plane and a radial distance of roughly 2.5 kpc from the center of the Galaxy. This places it within the Galactic bulge.

6. MODE CLASSIFICATION AND PULSATION PROPERTIES

The mode identification of the RR Lyrae stars in the field of M4 was based on the so-called Bailey diagram, i.e., the plot of brightness amplitude versus period (Fig. 8). In this plane, the RR Lyrae stars show a clear separation between FU and FO pulsators, and are also easily distinguished from other radial variables (Classical Cepheids, Type II Cepheids, Anomalous Cepheids, high amplitude delta Scuti stars). Fig. 8 shows that FO pulsators (cyan squares) have—as expected—shorter periods and smaller amplitudes than FU pulsators (red squares). The brightness amplitudes—again as expected—decrease monotonically when moving from the B (top panel) to the R (bottom panel) photometric band. Moreover, the FU amplitudes decrease steadily with increasing period. This trend has been attributed to the increasing efficiency of convective energy transport when moving from the hot to the cool edge of the FU-mode instability strip (Bono & Stellingwerf 1994; Bono et al. 1997b). The two labeled solid curves in the right side of the diagram represent the mean loci of FU variables of Oosterhoff classes I and II, as defined by Cacciari et al. (2005).

The candidate Blazhko RR Lyraes (black crosses) are all pulsating in the FU mode and they cover the entire period range of FU pulsators. The fraction of Blazhko stars is roughly 40% (13 out of 31), but recent space and ground measurements indicate that the fraction of RR Lyraes showing the Blazhko phenomenon is more typically of the order of 50% (Benkho et al. 2010; Jurcsik et al. 2009; Sódor et al. 2012; Kunder et al. 2013b). The vertical bars attached to the Blazhko crosses in Fig. 8 represent the modulation of the am-

plitude according to our photometry. They are preliminary estimates, since we have not performed a detailed analysis of the secondary modulation; better time series data than we presently have would be more suitable for that purpose. However, our data do indicate that the Blazhko amplitude generally decreases when moving from the hot to the cool edge of the fundamental-mode instability strip. In addition, we see a half dozen FU variables that, at fixed period, have larger brightness amplitudes (A_B, A_V) than the other RR Lyraes (i.e., placing them above/to the right of the OoI locus in the figure), including two of the Blazhko stars. This suggests a possible systematic difference between these stars and the bulk of the variables. We will find in the next section that a group of variables showing similar properties is also present in M5.

Variable V52 is characterized by very low amplitudes and a period ($P=0.8555$ d) significantly longer than the other low-amplitude FU pulsators. It is located close to the red edge of the instability strip (B – $R=1.33$ mag), and appears to be 0.20 mag brighter in V than the other RR Lyraes with similar B – R colors. This all suggests that V52 is well evolved from the zero-age horizontal branch.

In general, the FO pulsators have periods shorter than 0.4 days and amplitudes showing the typical bell (Bono et al. 1997b)—also sometimes called hairpin (Kunder et al. 2013c)—distribution represented by the solid curve in the left side of the Bailey diagram. The complete separation between FO and FU pulsators in this diagram is what allows us to classify them unambiguously. The new candidate member variable has a position in this diagram that is consistent with the previously known candidates. Three of the FO pulsators, including the new one, have very short periods and small amplitudes, suggesting that they are located close to the blue edge of the first overtone instability strip.

The Bailey diagram indicates that the RR Lyraes in M4 cover the entire width of the instability strip, but so far we lack any evidence of the presence of mixed-mode pulsators (Kunder et al. 2011).

Fig. 9 displays the light curves of a representative sample of first-overtone pulsators, while Fig. 10 shows the light curves of FU pulsators. From top to bottom, the RR Lyraes are ranked by increasing pulsation period; from left to right the different panels display the light curves in the U , B , V , R and I bands. The numbers in parentheses specify the number of points plotted, while IDs of the variables and the pulsation periods are given in the leftmost panel. Figs. 11 and 12 illustrate our near-infrared JHK data for the same stars.

We have also investigated the ratios between the brightness amplitudes as measured in the different optical bands. This diagnostic serves a double purpose: objects that show clear discrepancies in these ratios are likely to be either (a) other types of variable or (b) blended with other stars. For instance, theoretical pulsation models and empirical data indicate that the optical amplitude ratios of FU and FO Cepheids should be similar (Szabados & Dora 2012), but the same is not true for RR Lyraes (Kunder et al. 2013c). The data plotted in the top panel of Fig. 13 show that the ratio between the B - and V -band amplitudes in M4 maintains a quite stable value over the entire period range of the FU and FO variables. A similar result is found for the B - to R -band amplitude ratios (bottom panel), but here the spread is slightly larger (0.06 or 3.8% versus 0.03 or 2.3%). The lack of clear outliers is additional evidence of the “clean” nature of the RR Lyrae sample in M4.

Moreover, a comparison of the mean amplitude ratios in M4 with similar ratios for seven other Galactic globulars col-

lected by Kunder et al. (2013c) shows very good agreement (Fig. 14), within the errors, for both FO (blue squares) and FU (red squares) pulsators. Three out of the seven globulars are OoII clusters (NGC 7078, NGC 4590, M22) and the remaining four are OoI clusters (NGC 3201, NGC 1851, NGC 4147, NGC 6715). Note that the two outliers, NGC 3201 and NGC 6715, are both OoI clusters, but each has only a limited sample of FO variables: four and eight respectively. However, these Oosterhoff classifications should be treated with caution because both M4 and NGC 6715 could be considered Oosterhoff-intermediate, depending upon the classification diagnostic (either the mean period, or the (RRc):(RRab+RRc) population ratio) one chooses to adopt. In particular, the mean period of the entire sample of RR Lyraes in NGC 6715 is 0.60 d, i.e., intermediate between OoI and OoII, while for M4 it is 0.55 d, i.e., typical for OoI clusters. On the other hand, the population ratio for NGC 6715 is 0.14 (Sollima et al. 2010), i.e., typical for OoI clusters, while for M4 it is 0.30, i.e., intermediate between OoI and OoII clusters.

7. THE RR LYRAES IN M4 AND M5

To better interpret the pulsation properties of RR Lyraes in M4 we have made a detailed comparison with the RR Lyraes in M5 = NGC 5904. Accurate iron abundances based on high-resolution spectra give similar results for the two clusters: $[\text{Fe}/\text{H}] = -1.17 \pm 0.05$ (estimated systematic uncertainty) for M4 and -1.34 ± 0.06 for M5 (Carretta et al. 2009). Note that the mean iron abundance of M4 has been solidly confirmed by Malavolta et al. (2014) on the basis of medium-resolution spectra for $\sim 2,800$ stars collected with FLAMES/GIRAFFE at VLT. Specifically, they found $\langle [\text{Fe}/\text{H}] \rangle = -1.07$, $\sigma = 0.025$ (standard deviation, one star) for RGB stars and $\langle [\text{Fe}/\text{H}] \rangle = -1.16$, $\sigma = 0.09$ for subgiant and main-sequence stars. The available accurate spectroscopic measurements also indicate similar α -element abundances in M4 and M5 (Pritzl et al. 2004). Moreover, M5 is also affected by very low reddening ($E(B-V) = 0.03$, Harris 1996) and essentially no differential reddening, increasing its value as a reference standard.

It should also be noted that precise spectroscopic analysis has suggested that there are some differences in detail between the heavy-element mixes of the two clusters. For instance, Yong et al. (2008) state, among other conclusions, "... (2) the elements from Ca to Ni have indistinguishable compositions in M4 and M5, (3) Si, Cu, Zn, and all *s*-process elements are approximately 0.3 dex overabundant in M4 relative to M5, and (4) the *r*-process elements Sm, Eu, Gd, and Th are slightly overabundant in M5 relative to M4." However, the astrophysical significance of these minor differences—what they mean for the physical state of the environment in which the clusters formed, and how they have affected the evolutionary processes that occurred in the individual stars of the two clusters—are not fully understood. For our immediate purposes, it is sufficient that all the available evidence indicates that the overall abundances of elements heavier than helium, the theoreticians' Z , are the same for the two clusters within well under a factor of 2 (0.3 dex).

To quantify the comparison of the pulsation properties of the RR Lyraes in M4 and in M5, we considered two observables that are by their nature unaffected by reddening and extinction: the periods and brightness amplitudes of the variables. Fig. 15 shows that the period-frequency distributions in the two clusters are quite similar. The two samples differ in size by slightly more than a factor of two (45 versus 102), but

within the counting statistics they show very similar period distributions. In particular, each displays two well separated peaks: one for FO pulsators, at $P \sim 0.3$ d, and one for FU, at $P \sim 0.5$ d. More quantitatively, we find that the FU pulsators in the two clusters have identical mean periods (0.55 d). The same conclusion comes from the RR Lyrae population ratios, i.e., the ratio of the number of FOs to the total number of RR Lyraes: we find that (RRc):(RRab+RRc) is 0.30 for both M4 and M5.

The Bailey diagram for M5 (Fig. 16), which is inherently reddening- and extinction-independent on both its axes, is also qualitatively very similar to that of M4 (Fig. 8 above).

To further quantify the comparison between the helium-burning phases of stars in M4 and M5, we decided to extend the comparison to the entire horizontal branch. We adopted the HB parameter introduced by Lee et al. (1994): $\tau_{\text{HB}} = (B-R)/(B+V+R)$, where roman B, V and R indicate the number of HB stars bluer than the RR Lyrae stars, the number of RR Lyraes and the number of HB stars redder than the RR Lyraes (not to be confused with italic *B*, *V* and *R*, which represent photometric bandpasses). Recent estimates of τ_{HB} for both M4 and M5 (Castellani et al. 2013, in preparation) indicate that the HB morphology in the above clusters is similar (0.24 versus 0.37 on a scale of -1.0 to $+1.0$) and spans the entire flat region of the HB. This indicates that red giant branch stars in the two clusters must have experienced very similar mass loss rates. On the other hand, the HB morphology of the Oosterhoff-intermediate cluster NGC 6715, is significantly bluer ($\tau_{\text{HB}} = 0.87$), suggesting that the mass loss rate in this slightly more metal-poor cluster ($[\text{Fe}/\text{H}] \approx -1.6$) was more efficient than in M4 and M5. These findings suggest that the simultaneous comparison of observed RR Lyrae period distributions and HB morphologies can provide new constraints for theories of the late stages of stellar evolution (Dotter 2008; VandenBerg et al. 2013). Particularly and importantly, we can begin to consider whether the so-called second-parameter problem and the Oosterhoff dichotomy might be two sides of the same coin (Bono et al. 1997a).

In this context it is worth recalling once again that Galactic globular clusters hosting sizable samples of RR Lyraes can be divided into two groups according to the pulsation properties of the variables: Oosterhoff type I (OoI) clusters are characterized by mean FU periods $\langle P \rangle \sim 0.55$ d, and population ratios (RRc):(RRab+RRc) ~ 0.17 , while the Oosterhoff type II (OoII) clusters have longer mean periods, $\langle P \rangle \sim 0.65$, and larger FO populations, (RRc):(RRab+RRc) ~ 0.44 . According to this classification both M4 and M5 appear to be OoI clusters on the basis of the mean period and OoI-intermediate on the basis of the pulsation-mode population ratio. It is also worth mentioning here that the brightness amplitudes plotted in Figs. 8 and 16 support the interpretation that both M4 and M5 are OoI clusters. The two black lines toward the right side of each figure display the typical loci of OoI and OoII clusters according to Cacciari et al. (2005), while the "hairpin" black lines toward the left side of the figures display the mean locus for FO pulsators in 14 OoII GCs according to Kunder et al. (2013c). We still lack an analytical relation for FO pulsators in OoI GCs due to their much smaller numbers, but the systematic offset of the RRc variables in both M4 and M5 from the OoII locus suggests, once again, a non-OoII nature for the RR Lyraes in both clusters.

During the last few years, evidence has mounted that GGCs for which the census of RR Lyrae stars is either complete

or approaching completeness display this “neutral Oo status” (Kunder et al. 2013a,b) if the Bailey diagram, the period distributions, and the population ratios are all taken into account (Catelan et al. 2010).

8. SUMMARY AND CONCLUSIONS

We have presented optical and near-infrared *UBVRIJHK* photometry of the Galactic globular cluster M4 (NGC 6121), with particular emphasis on the RR Lyrae variable stars in the cluster. We have made a particular effort to accurately reidentify the previously discovered variables, and have been fortunate to discover two new probable RR Lyrae variables in the M4 field: by their positions on the sky and their photometric properties one is a probable member of the cluster and the other is a probable background (bulge?) object. We conclude that Clement’s star V17 is probably in fact V52 with an incorrectly reported position, and that the previously reported period estimate for V52 was in error. We have also provisionally reidentified and published accurate positions for three RR Lyrae candidates previously identified only in finding charts.

For the convenience of future researchers we have published accurate equatorial coordinates for all 47 candidate RR Lyrae stars, new mean magnitudes for 46 of them, and new period estimates for 45. We have also included positions and mean photometry for 39 candidate variable stars of other types, including 34 previously identified in the literature and five newly discovered here. For 18 of these we are not able to confidently confirm variability or estimate periods; in some cases this is due to limitations of our time sampling, in others it is because the stars are not really variable. For the remaining 22, most of which are probably eclipsing binaries, we do

provide new period estimates.

We have illustrated optical and near infrared color-magnitude diagrams for the cluster and have shown the locations of the variable stars in them. We have presented the Bailey (period-amplitude) diagrams and the period-frequency histograms for M4 and have compared them to the corresponding diagrams for M5. We conclude that the RR Lyrae populations in the two clusters are quite similar in all the characteristic properties that we have considered. The mean periods, pulsation-mode ratios, and Bailey diagrams of these two clusters show support for the recently proposed “Oosterhoff-neutral” classification.

Our calibrated photometry for M4, a finding chart, equatorial and pixel coordinates for all stars, and light-curve data for the variable candidates are all available from our web site. These astronomical data will also be the raw material for more detailed astrophysical analyses of the physical nature of the RR Lyraes in M4 and of the cluster itself, in the global context of the formation and evolution of the Galactic halo. These papers are currently in preparation.

It is a pleasure to thank John Grula, the Librarian of the Carnegie Observatories, for providing us several papers that were not available on ADS. This work was partially supported by PRIN–INAF 2011 “Tracing the formation and evolution of the Galactic halo with VST” (P.I.: M. Marconi) and by PRIN–MIUR (2010LY5N2T) “Chemical and dynamical evolution of the Milky Way and Local Group galaxies” (P.I.: F. Matteucci). PBS is pleased to acknowledge financial support from the Erasmus Mundus-AstroMundus Consortium of Universities. G.B. thanks The Carnegie Observatories visitor programme for support as a science visitor.

APPENDIX

NOTES ON INDIVIDUAL RR LYRAE STARS

V1 – The *B*, *V* and *R* light curves show a few data points out of phase. The mean magnitudes and the amplitudes are minimally affected.

V2 – Small amplitude modulations in the *B*- and *V*-band light curves indicate that V2 might be a candidate Blazhko variable. The mean *U*, *I* magnitudes and their amplitudes are based on Sturch (1977), Cacciari (1979), and Liu & Janes (1990) for the *U*-band data and on Clementini et al. (1994) for the *I*-band data.

V3 – The current photometry covers only the phases around maximum (increasing and decreasing branch). The *B*-band amplitude is based on data from (Clement et al. 2001).

V6 – The mean *U*-band magnitude and amplitude are based on data from Cacciari (1979).

V7 – The current A_V amplitude is smaller than than previous estimates (1.06 versus 1.24). The difference might be due to the fact that the period of V7 is close to 0.5 d.

V11 – Amplitude estimates in all bands are affected by very large Blazhko modulation. The mean *U*-band magnitude and amplitude are based on data from Sturch (1977).

V12 – The mean *U*-band magnitude and amplitude are based on data from Sturch (1977).

V14 – Very small amplitude modulations only visible in the *B*-band light curve suggest that V14 might be a Blazhko variable. The mean *U*-band magnitude and amplitude (A_U) are based on data from Sturch (1977) and Cacciari (1979).

V15 – Amplitude modulations in the *B*-, *V*- and *R*-band light curves indicate that V15 is a candidate Blazhko variable. According to Clementini et al. (1994), this is a peculiar variable with a decreasing period and either a strong Blazhko effect or a pulsation mode switching from FU to FO. The behavior resembles the RR Lyrae V79 in M3 Goranskij (1980). The *B*- and *V*-band light curves show a larger amplitude modulation than in the *R* band.

V18 – We confirm that this is an FU mode RR Lyrae.

V19 – The mean *U*-band magnitude and amplitude are based on data from Sturch (1977).

V21 – The current *B*-, *V*- and *R*-band amplitudes are smaller than previous estimates, probably due to the fact that the pulsation period is close to 0.5 d.

V22 – Amplitude modulations in the *B*- and *V*-band light curves indicate that V22 is a candidate Blazhko variable.

V24 – Amplitude modulations in the *B*-, *V*- and *R*-band light curves indicate that V24 is a candidate Blazhko variable.

V27 – The mean *U*-band magnitude and amplitude are based on data from Sturch (1977) and Cacciari (1979).

V28 – Amplitude modulations in the *B*-, *V*- and *R*-band light curves indicate that V28 is a candidate Blazhko variable. The

mean U -band magnitude and amplitude are based on data from Sturch (1977).

V29 – Small amplitude modulations in the B - and V -band light curves suggest that V29 may be a candidate Blazhko variable. The period, the mean magnitudes, the amplitudes and the epoch of maximum include data from Sturch (1977), Cacciari (1979) and Clementini et al. (1994).

V30 – The mean U -band magnitude and amplitude are based on data from Cacciari (1979).

V31 – Amplitude modulations in the B -, V - and R -band light curves indicate that V31 is a candidate Blazhko variable. The mean U -band magnitude and amplitude are based on data from Sturch (1977).

V32 – The period, the mean magnitudes, the amplitudes and the epoch of maximum include data from Sturch (1977), Cacciari (1979) and Liu & Janes (1990).

V33 – The period, the mean magnitudes, the amplitudes and the epoch of maximum include data from Sturch (1977), Cacciari (1979) and Liu & Janes (1990) for the U , B , and V bands and from Liu & Janes (1990) for the R and I bands.

V34 – Limited number of data points in all bands.

V35 – Moderate amplitude modulations in the B -, V - and R -band light curves indicate that V35 is a candidate Blazhko variable. The mean U -band magnitude and amplitude are based on data from Sturch (1977) and Cacciari (1979).

V36 – Somewhat noisy light curves.

V38 – The B - and the V -band light curves show small amplitude modulations. It might be a plausible candidate to have been or to be becoming a Blazhko variable.

V39 – Amplitude modulations in the B -, V - and R -band light curves indicate that V39 is a candidate Blazhko variable.

V42 – The period, the mean magnitudes, the amplitudes and the epoch of maximum include data from Cacciari (1979) and Clementini et al. (1994).

V43 – The astrometry is from Clement et al. (2001). The photometric parameters are based on data from Cacciari (1979).

V49 – This is a low-amplitude FO variable with a very short period. The light curves are noisy but its color is among the bluest of the entire sample.

V64 – Amplitude modulations in the B -, V - and R -band light curves indicate that V64 is a candidate Blazhko variable. This is V45 in Kaluzny et al. (1997). This is clearly a distant background object unrelated to M4.

C1 – New cluster FO variable.

C2 – New candidate field FU variable, a background object unrelated to M4.

According to our current photometric results these candidate RR Lyrae variables listed in the Clement et al. (2001) catalog, do not seem to be variables: V17, V44, V45, V46, V47, V48, V50, and V51. For the candidate variable V34 we have strong evidence of RR Lyrae-like variability, but do not have enough phase points to determine a period or define a light curve. For V43 we have only astrometric information and no new calibrated photometry of our own.

REFERENCES

- Akhter, S., Da Costa, G. S., Keller, S. C., & Schmidt, B. P. 2012, *ApJ*, 756, 23
- Bassa, C. et al. 2004 *ApJ*, 609, 755
- Benkho, J. M., et al. 2010, *MNRAS*, 409, 1585
- Bono, G., Caputo, F., Cassisi, S., Incerpi, R., & Marconi, M. 1997, *ApJ*, 483, 811
- Bono, G., Caputo, F., Castellani, V., & Marconi, M. 1997, *A&AS*, 121, 327
- Bono, G., & Stellingwerf, R. F. 1994, *ApJS*, 93, 233
- Cacciari, C. 1979, *AJ*, 84, 1542
- Cacciari, C., Corwin, T. M., & Carney, B. W. 2005, *AJ*, 129, 267
- Cardelli, J. A., Clayton, G. C., & Mathis, J. S. 1989, *IAUS*, 135, 5
- Carretta, E., Bragaglia, A., Gratton, R., D'Orazi, V., & Lucatello, S., 2009, *A&A*, 508, 695
- Catelan, M., Valcarce, A. A. R., & Sweigart, A. V., 2010, in *IAU Symp. 266, Star Clusters: Basic Galactic Building Blocks throughout Time and Space*, 281
- Clement, C. M., et al. 2001, *AJ*, 122, 2587
- Clementini, G., Merighi, R., Pasquini, L., Cacciari, C., & Gouffes, C. 1994, *MNRAS*, 267, 83
- Coppola, G., et al. 2011, *MNRAS*, 416, 1056
- de Sitter, A. 1947, *BAN*, 10, 287
- Djorgovski, S. G., et al. 2011, *ArXiv e-prints*, arXiv:1102.5004
- Dotter, A., 2008, *ApJ*, 687, L21
- Drake, A. J., et al. 2009, *ApJ*, 696, 870
- Freedman, W., et al. 2012, *Spitzer Proposal*, 90002
- Shimasaku, K., & Schneider, D. P. 1996, *AJ*, 111, 1748
- Gezari, S., et al. 2013, *ApJ*, 766, 60
- Goranskij, V. P. 1980 *ATsir*, 1111, 6
- Greenstein, J. L. 1939 *ApJ*, 90, 401
- Hansen, B. M. S., et al. 2004, *ApJS*, 155, 551
- Harris, W. E. 1996, *AJ*, 112, 1487
- Hendricks, B. Stetson, P. B., VandenBerg, D. A., & Dall'Ora, M. 2012, *AJ*, 144, 25
- Ivans, I. I., Sneden, C., Kraft, R. P., Suntzeff, N. B., Smith, V. V., Langer, G. E., & Fulbright, J. P. 1999, *AJ*, 118, 1273
- Jurcsik, J., et al. 2009, *MNRAS*, 400, 1006
- Kaluzny, J., Thompson, I. B., Krzeminski, W., Pych, W., Rucinski, S. M., Burley, G. S., & Shectman, S. A. 1997, *AJ*, 113, 2219
- Kaluzny, J., Thompson, I. B., Rozycka, M., Dotter, A., & Krzeminski, W. 2013, *AJ*, 145, 43
- Kaluzny, J., Thompson, I. B., Rozycka, M., & Krzeminski, W. 2013, *AcA*, 63, 181
- Kinemuchi, K., Smith, H. A., Woźniak, P. R., McKay, T. A., & ROTSE Collaboration. 2006, *AJ*, 132, 1202
- Kunder, A., et al. 2011, *AJ*, 141, 15
- Kunder, A., Salaris, M., Cassisi, S., De Propriis, R., Walker, A., Stetson, P. B., Catelan, M., & Amigo, P. 2013, *AJ*, 145, 25
- Kunder, A., et al. 2013, *AJ*, 145, 33
- Kunder, A., et al. 2013, *AJ*, 146, 119
- Landolt, A. U. 1973, *AJ*, 78, 959
- Landolt, A. U. 1983, *AJ*, 88, 439
- Landolt, A. U. 1992, *AJ*, 104, 340
- Layden, A. C. 1998, *AJ*, 115, 193
- Lee, Y.-W., Demarque, P., & Zinn, R. 1994, *ApJ*, 423, 248
- Libralato, M., Bellini, A., Bedin, L. R., Piotto, G., Platais, I., Kissler-Patig, M., & Milone, A. P. 2014, *A&A* accepted, arXiv:1401.3344
- Liu, T., & Janes, K. A. 1990, *ApJ*, 360, 561
- Lyne, A. G., Biggs, J. D., Brinklow, A., McKenna, J., & Ashworth, M. 1988 *Nature*, 332, 45
- Malavolta, L., Sneden, C., Piotto, G., Milone, A. P., Bedin, L. R., & Nascimbeni, V. 2014, *AJ*, 147, 25
- Marchetti, E. et al. 2006, *SPIE*, 6262, 21
- Marino, A. F., Villanova, S., Piotto, G., Milone, A. P., Momany, Y., Bedin, L. R., & Medling, A. M. 2008, *A&A*, 490, 625
- McCall, M. L. 2004, *AJ*, 128, 2144
- Miceli, A., et al. 2008, *ApJ*, 678, 865
- Milone, A. P., et al. 2014, *MNRAS* accepted, arXiv:1401.1091
- Mochejska, B. J., Kaluzny, J., & Thompson, I., Pych, W. 2002, *AJ*, 124, 1486
- Monelli, M., et al. 2013, *MNRAS*, 431, 2126
- Mucciarelli, A., Salaris, M., Lovisi, L., Ferraro, F. R., Lanzoni, B., Lucatello, S., & Gratton, R. G. 2011, *MNRAS*, 412, 81

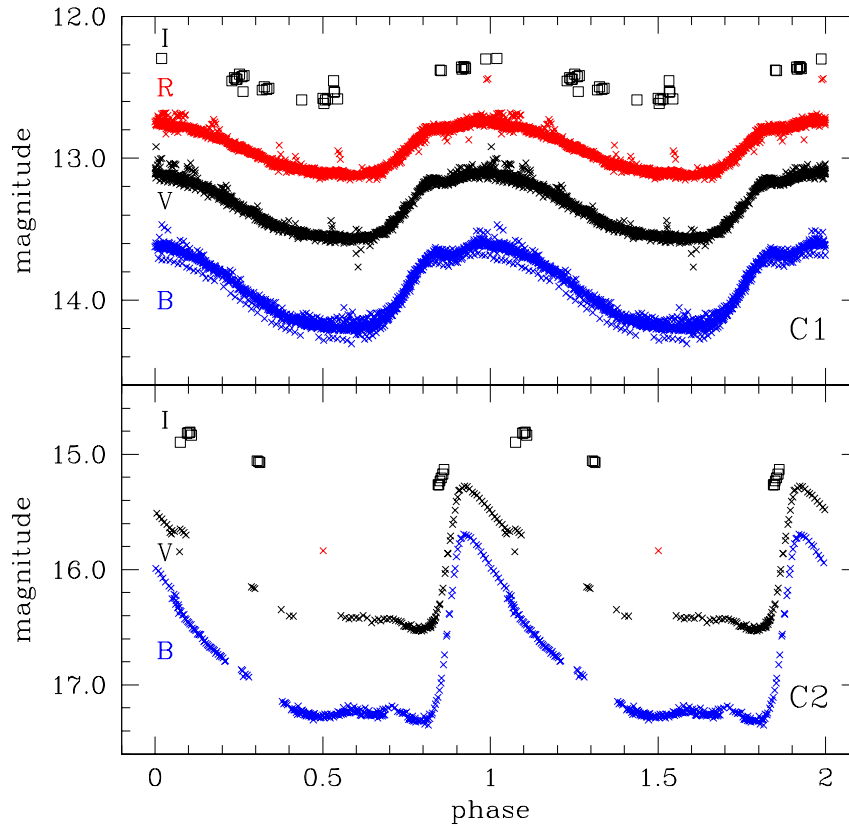


Fig. 1.— Optical light curves for newly identified RR Lyrae candidates C1 (upper) and C2 (lower). The blue, black, and red points represent observed magnitudes in the *B*, *V*, and *R* photometric bands, respectively. Empty black squares are measurements in the *I* band. The stars' estimated periods are: (C1) 0.2863 d and (C2) 0.4548 d.

- Palaversa, L., et al. 2013, *AJ*, 146, 101
 Pojmanski, G. 2002, *AcA*, 52, 397
 Pritzl, B. J., Venn, K. A., & Irwin, M. 2004, *AJ*, 130, 2140
 Scargle, J. D. 1982, *ApJ*, 263, 835
 Schlegel, D. J., Finkbeiner, D. P., & Davis, M. 1998, *ApJ*, 500, 525
 Sigurdsson, S., Richer, H. B., Hansen, B. M., Stairs, I. H., & Thorsett, S. E. 2003, *Science*, 301, 193
 Sódor, Á., et al. 2012, *MNRAS*, 427, 1517
 Sollima, A., Cacciari, C., Bellazzini, M., & Colucci, S., 2010, *MNRAS*, 406, 329
 Stellingwerf, R. F. 2011, *RR Lyrae Stars, Metal-Poor Stars, and the Galaxy*, Carnegie Observatories Astrophysics Series, Vol. 5, 74
 Stetson, P. B. 1987, *PASP*, 99, 191
 Stetson, P. B. 1989, in "Image and Data Processing; Interstellar Dust," V Escola Avançada de Astrofísica, Departamento de Astronomia, Instituto Astronômico e Geofísico, Universidade de São Paulo, p. 1
 Stetson, P. B. 1996, *PASP*, 108, 851
 Stetson, P. B. 2000, *PASP*, 112, 925
 Stetson, P. B. 2005, *PASP*, 117, 563
 Stetson, P. B., et al. 1998, *ApJ*, 508, 491
 Sturch, C. R. 1977, *PASP*, 89, 349
 Szabados, L., & Dóra, N. 2012, *MNRAS*, 426, 3148
 Szeidl, B., Hurta, Z., Jurcsik, J., Clement, C., & Lovas, M. 2011, *MNRAS*, 411, 1744
 VandenBerg, D. A., Brogaard, K., Leaman, R., & Casagrande, L. 2013, *ApJ*, 775, 134
 Vivas, A. K., et al. 2004, *AJ*, 127, 1158
 Welch, D. L., & Stetson, P. B. 1993, *AJ*, 105, 1813
 Yao, B.-A. 1977, *Acta Ast Sin*, 18, 216
 Yong, D., Karakas, A. I., Lambert, D. L., Chieffi, A., & Limongi, M. 2008, *ApJ*, 689, 1031

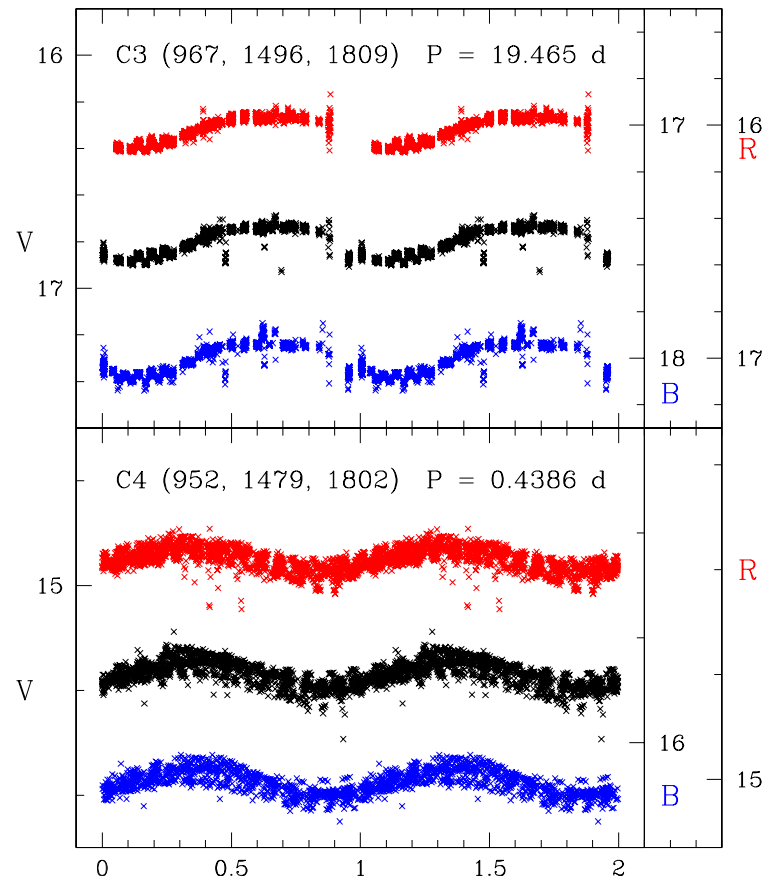


FIG. 2.— Optical light curves for newly identified variable candidates C3 (upper) and C4 (lower). The blue, black, and red points represent observed magnitudes in the *B*, *V*, and *R* photometric bands, respectively. Corresponding ordinate axes are labeled in the same colors. The legend gives the number of observations in each filter and the period for each star. Tick marks in the lower plot are separated by 0.20 mag.

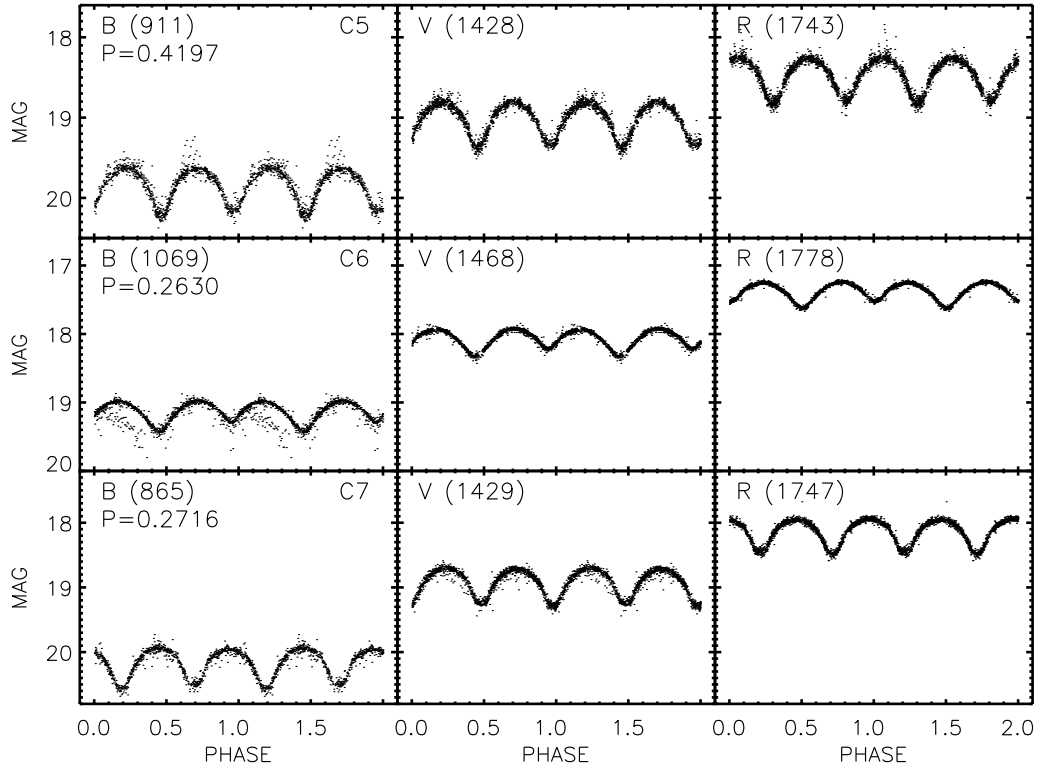


FIG. 3.— Optical light curves for the newly identified variable candidates C5 (top), C6 (middle), and C7 (bottom) in the *B* (left), *V* (middle), and *R* (right) photometric bandpasses.

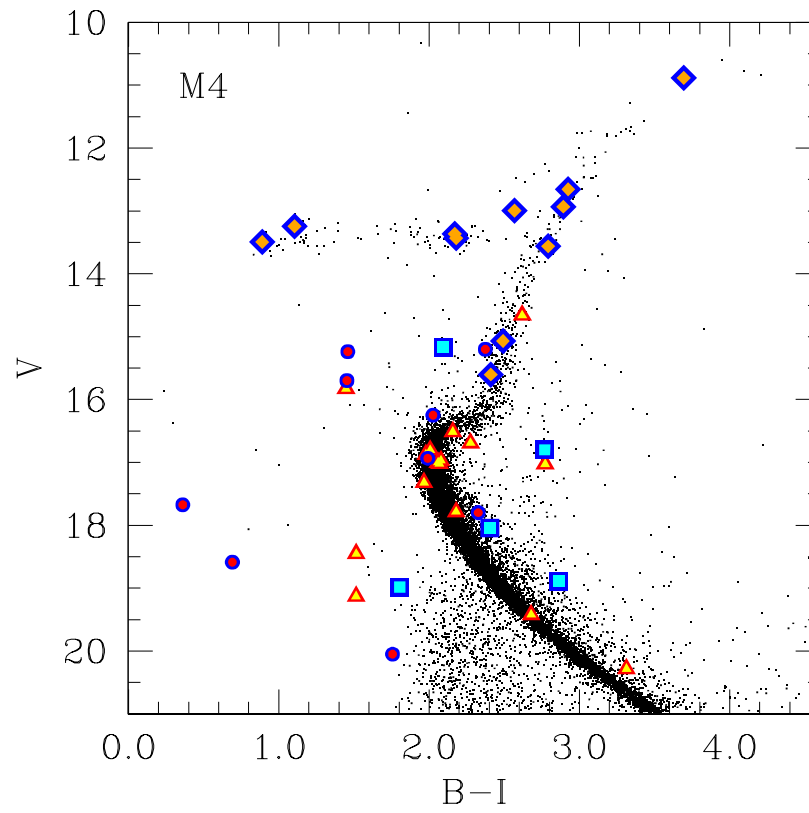


FIG. 4.— A V versus $B-I$ color-magnitude diagram for M4, with the variable candidates *not* of the RR Lyrae type illustrated as colored symbols. The red-and-yellow triangles represent the candidate variables of Kaluzny et al. (1997, 2013a and 2013b) for which we are able to recover the published periods from our data. The blue-and-red circles are for Kaluzny stars whose variability we are unable to confirm. The blue-and-cyan squares represent the five newly discovered candidates C3 through C7. Finally, the large blue-and-orange lozenges are for the remaining stars without Kaluzny designations (V53–60, V75, V79 and V80) where we are unable to confirm the variability.

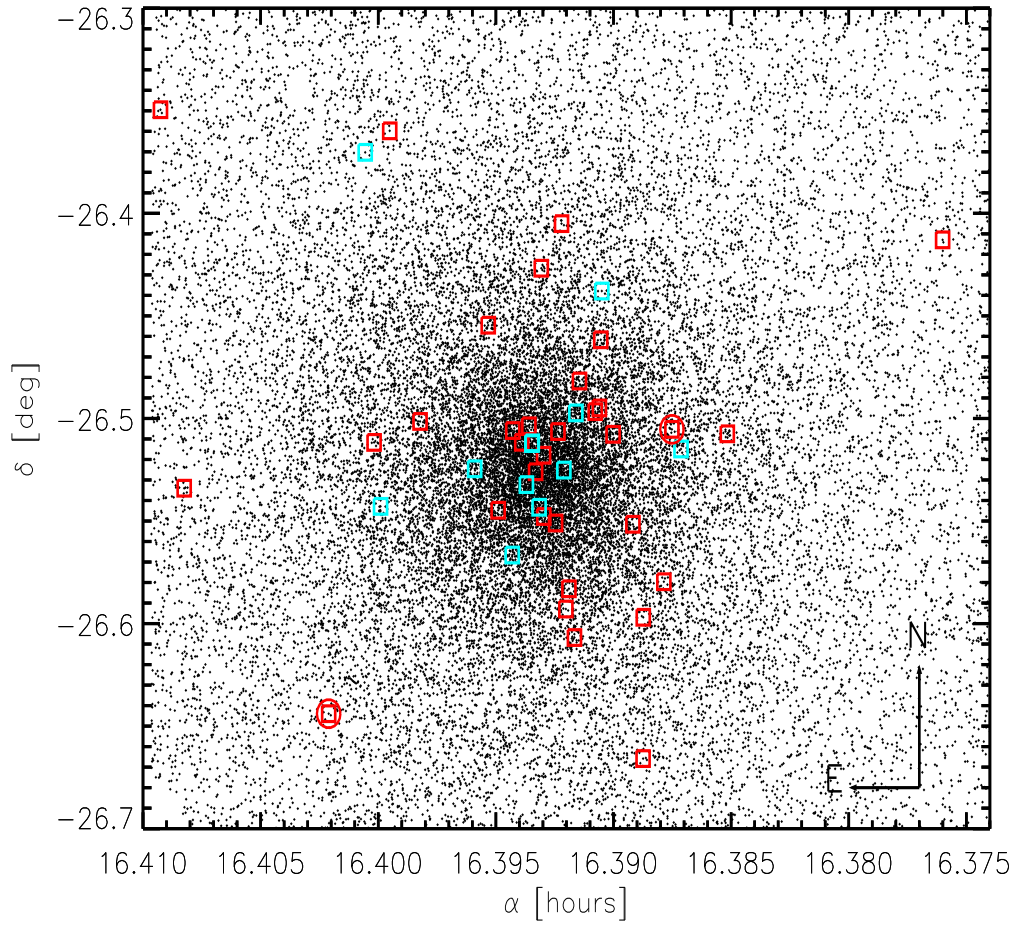


FIG. 5.— Distribution on the sky of RR Lyrae stars in the M4 field for which we have accurate optical and astrometric measurements. The sky area covered by our photometry is $35' \times 35'$. The red and cyan squares show the positions of fundamental and first overtone variables. Two probable field stars are circled. Note that eclipsing binaries, candidate long-period variables, and other variable types are not marked here.

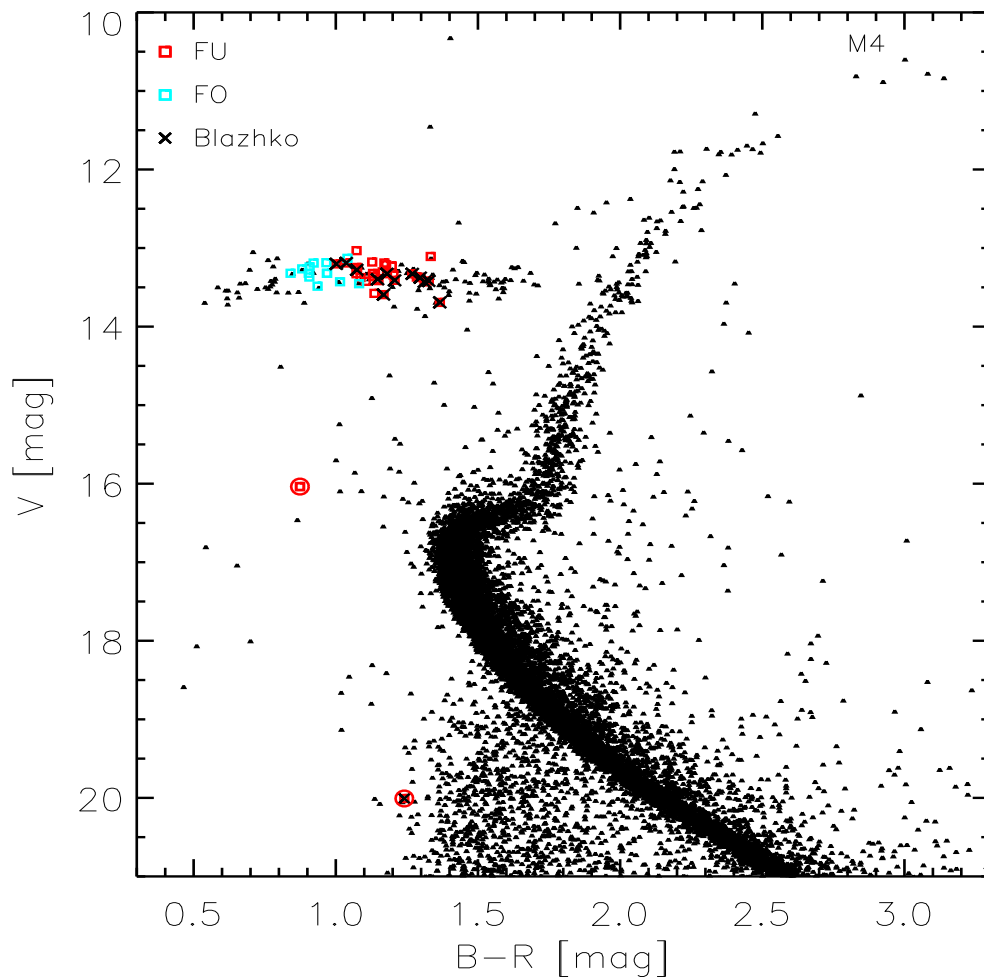


FIG. 6.— Optical ($V, B-R$) color-magnitude diagram for the M4 field. RR Lyrae variables pulsating in the fundamental (FU) or in the first overtone (FO) are represented by red and cyan squares, respectively. Black crosses identify candidate Blazhko stars. Two probable field stars are circled. Numerous field stars with $B-R \gtrsim 1.3$ are seen below the cluster main sequence.

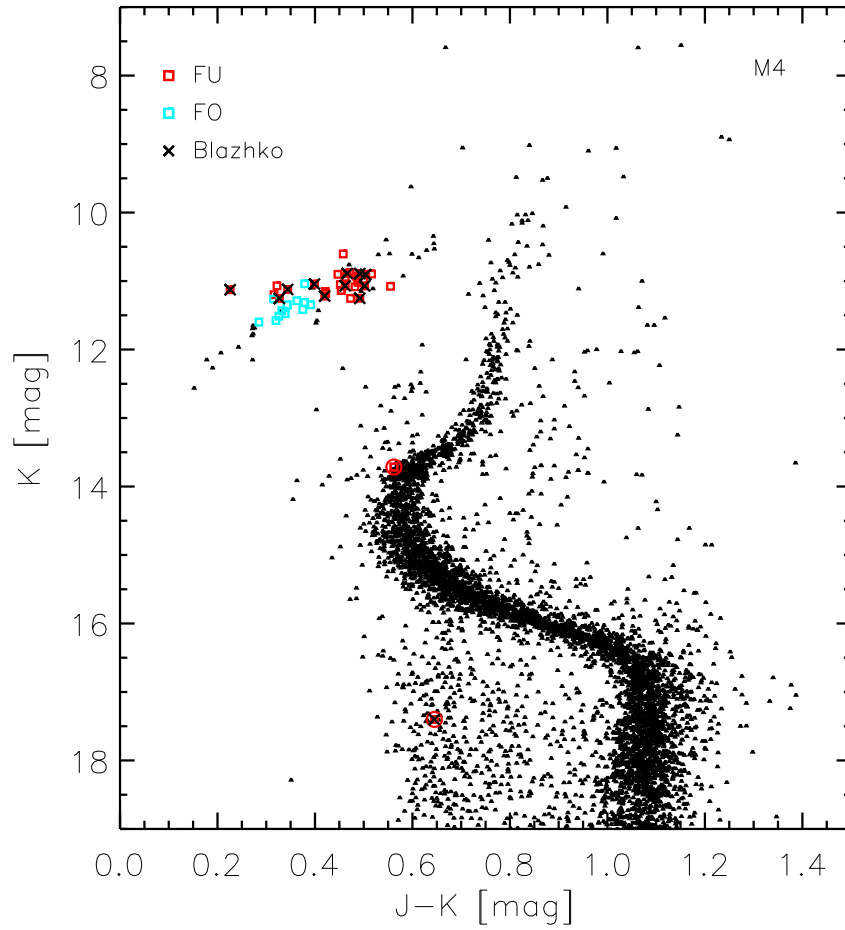


FIG. 7.— Near-infrared ($K, J-K$) color-magnitude diagram for the M4 field. RR Lyrae variables pulsating in the fundamental mode (FU) or in the first overtone (FO) are marked with red and cyan squares, respectively. The black crosses designate candidate Blazhko RR Lyrae stars. The two candidate field RR Lyrae stars are located at $K \sim 13.8$ and $K \sim 17$ mag. The field stars show a well defined blue edge with colors ranging from $J-K=0.6$ to $J-K=1.2$.

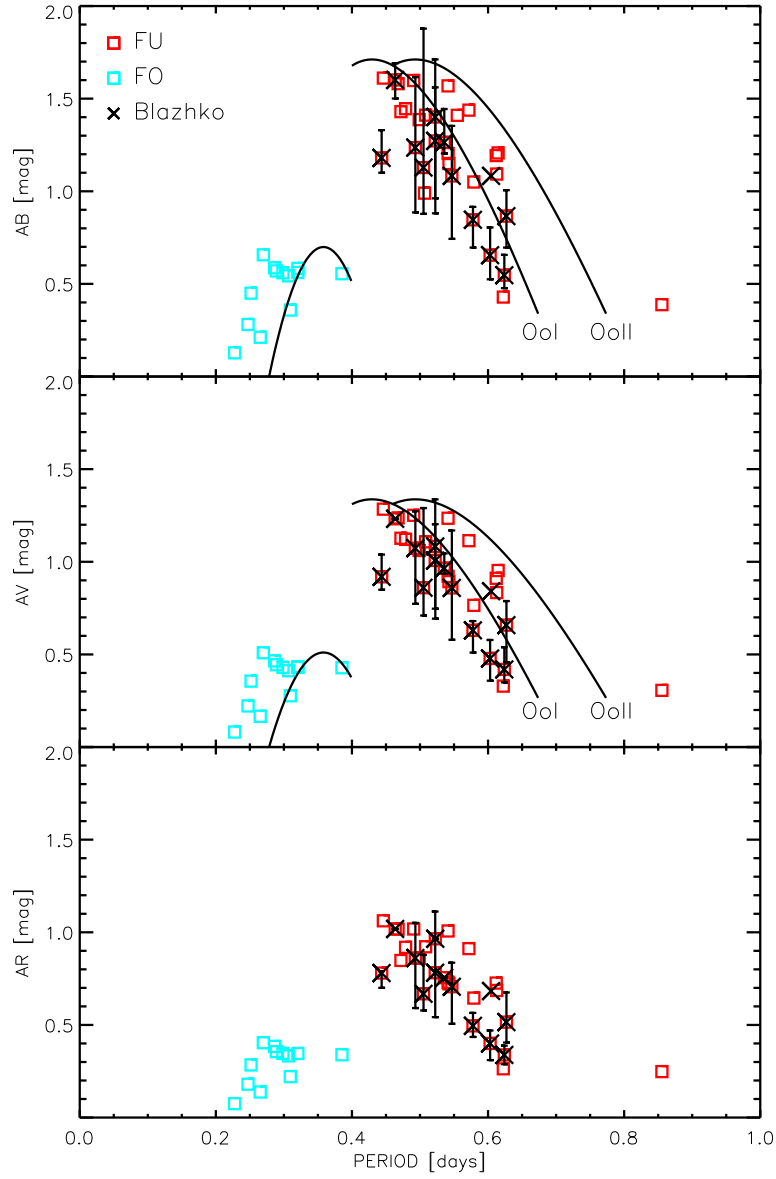


FIG. 8.— Top: A plot of the B -band amplitude versus period for RR Lyrae stars in M4 (Bailey diagram). Fundamental and first overtone RR Lyraes are plotted as red and cyan squares. Candidate Blazhko stars are marked with a black cross and the vertical bars display their range in brightness amplitude. Middle: Same as the top, but for the V -band amplitude. Bottom: Same as the top, but for the R -band amplitude.

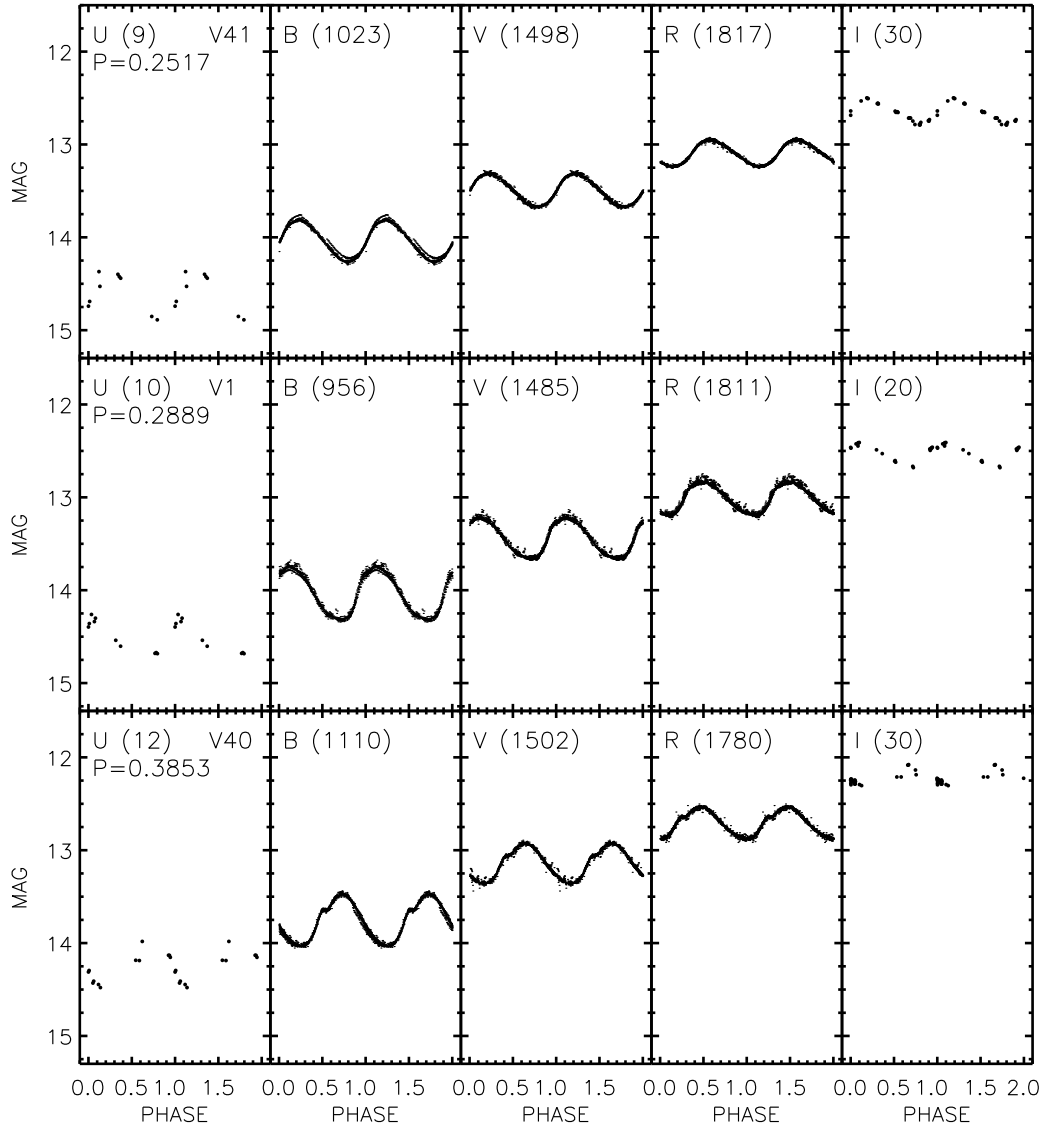


FIG. 9.— Optical light curves for some of the first overtone RR Lyrae stars in M4. From top to bottom the panels display the light curves of different variables ordered by increasing period. From left to right the different panels display the light curves in the *U*, *B*, *V*, *R* and *I* bands. The numbers in parentheses give the number of individual measurements per band. The identification numbers of the variables are given in the top right corner of the leftmost panel. The complete atlas of FO light curves is available in the electronic edition.

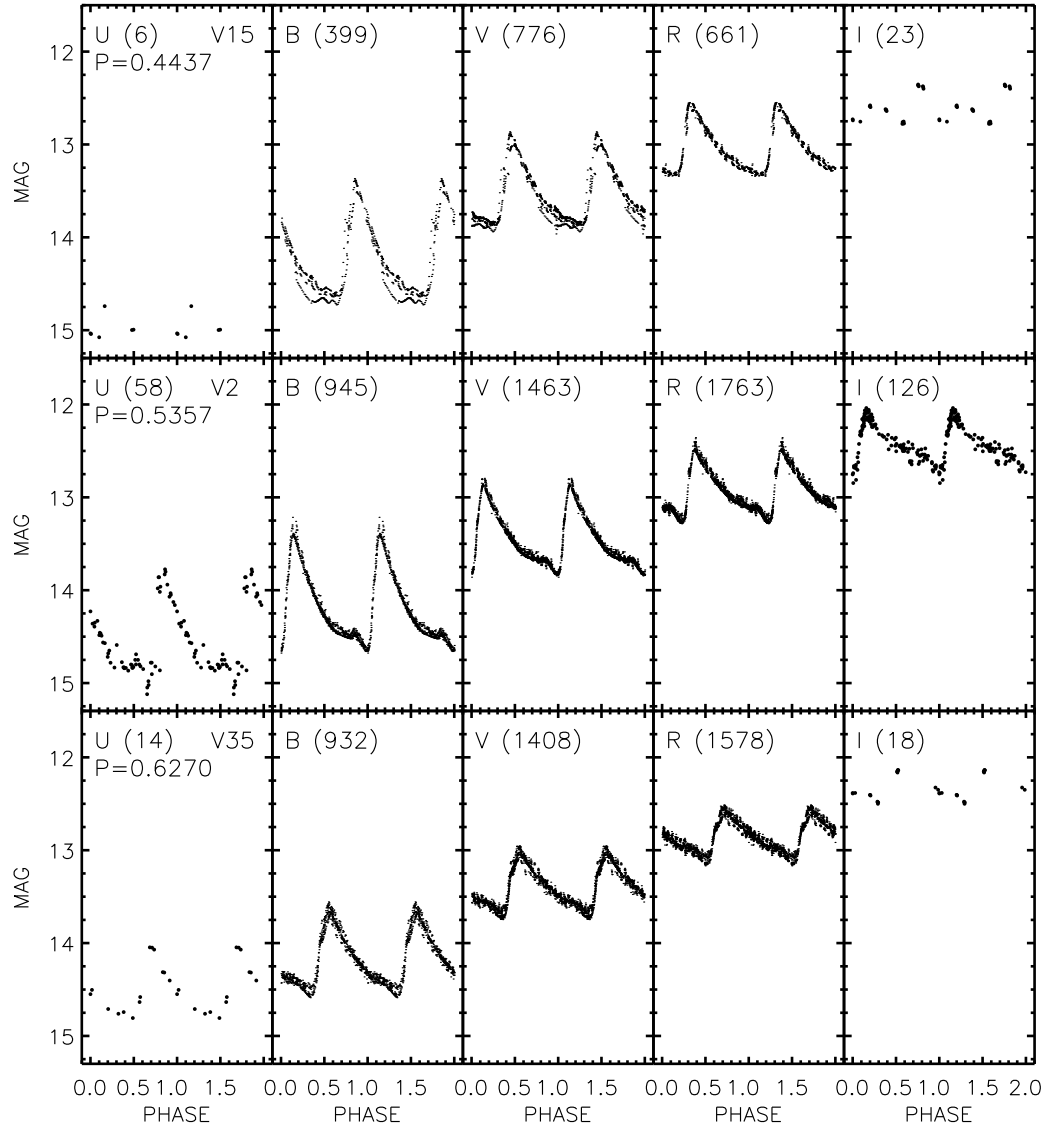


FIG. 10.— Same as Fig. 9, but for fundamental pulsators. The complete atlas of the FU light curves is available in the electronic edition.

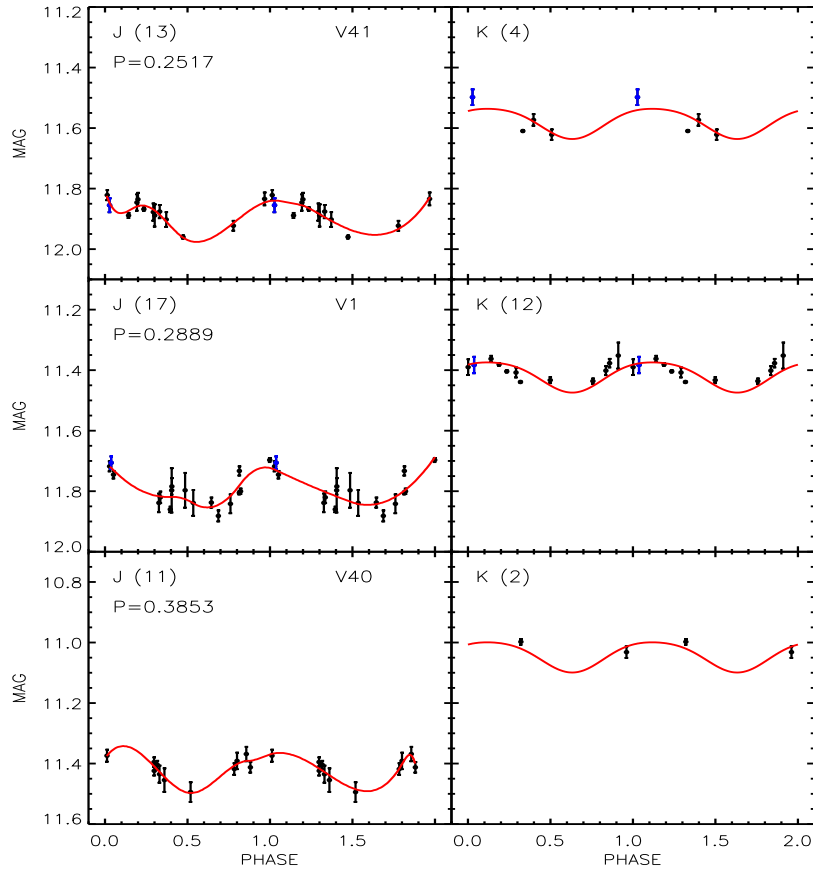


FIG. 11.— Near-infrared light curves for the same first overtone (FO) RR Lyrae stars as in Fig. 9. From top to bottom, the panels display the light curves of different variables ordered by increasing period. The left and the right panels display the light curves in the J and K bands. The numbers in parentheses report the number of individual measurements per band. The blue dots show the phase points based on 2MASS photometry. The vertical error bars display the standard deviation of the averaged phase points, while the red curves in the right panels show the fitted template light curves (see text for more details). The complete atlas of FO NIR light curves is available in the electronic edition.

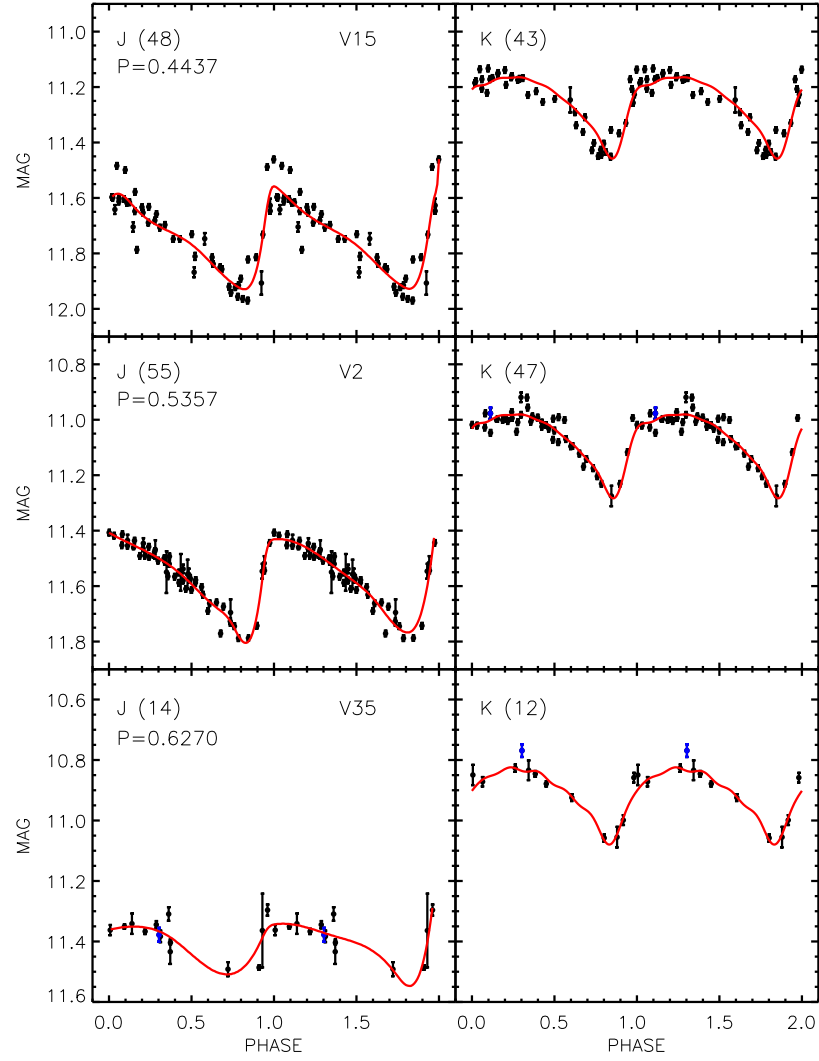


FIG. 12.— Same as Fig. 11, but for fundamental pulsators. The complete atlas of the FU NIR light curves is available in the electronic edition.

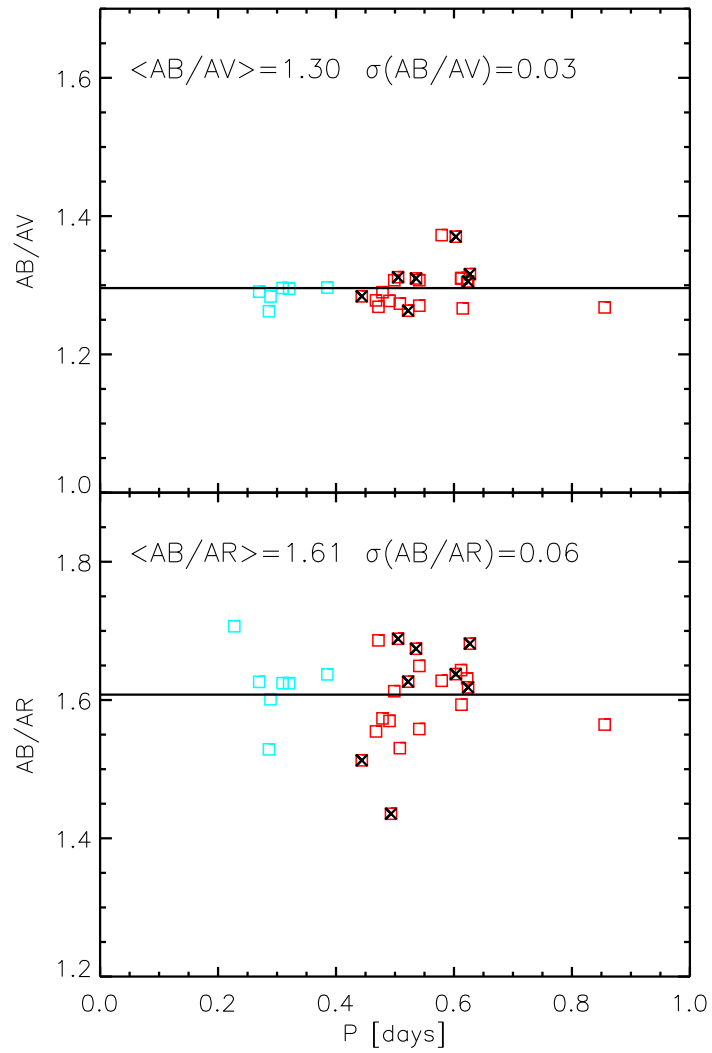


FIG. 13.— Top: Ratio between B - and V -band amplitudes for FU (red squares) and FO (cyan squares) variables as a function of period. The black crosses mark candidate Blazhko RR Lyraes. The horizontal black line shows the mean value of the ratio. Bottom: Same as the top, but for the B - versus R -band amplitude ratio.

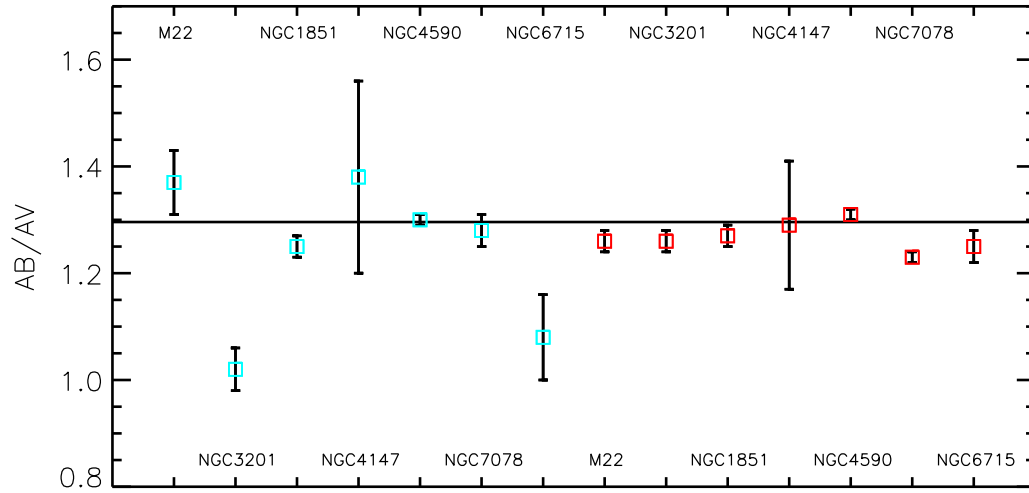


FIG. 14.— Mean values of the B - and V -band amplitude ratio for RR Lyrae stars in the sample of globulars collected by Kunder et al. (2013c) (see their Table 3 and 4). The mean amplitude ratios for FO (cyan squares) and FU (red squares) and their error bars as given by Kunder et al. are plotted at arbitrary periods. The horizontal solid line indicates the value of this ratio that we have measured in M4.

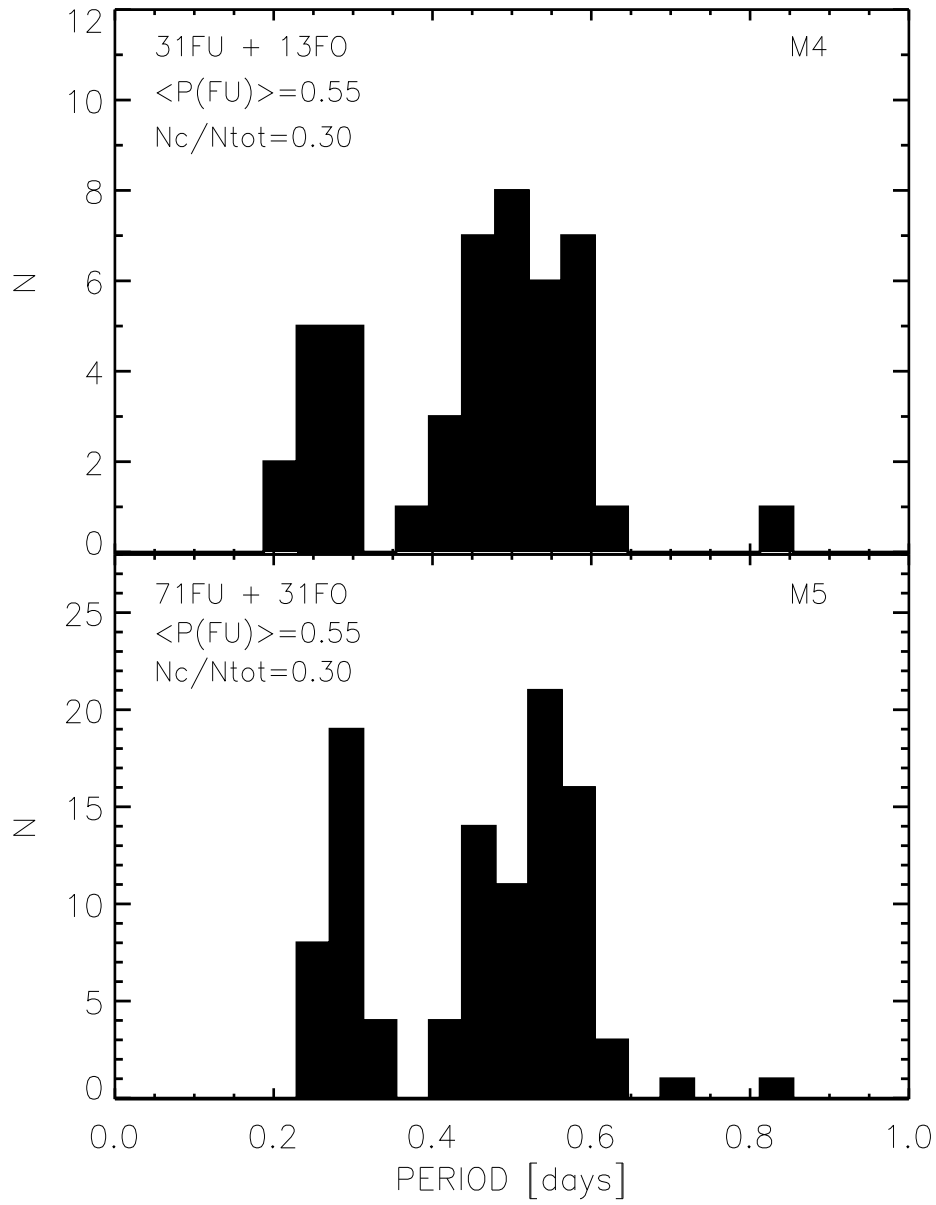


FIG. 15.— Top: Period distribution for RR Lyrae stars in M4. The legend gives the actual numbers of fundamental and first overtone pulsators, the mean period of the FU pulsators, and the ratio of the number of RRc-type (FO) pulsators to the total number of RR Lyraes (N_c/N_{tot}). See text for more details. Bottom: Same as the top, but for RR Lyraes in M5 (Coppola et al. 2011).

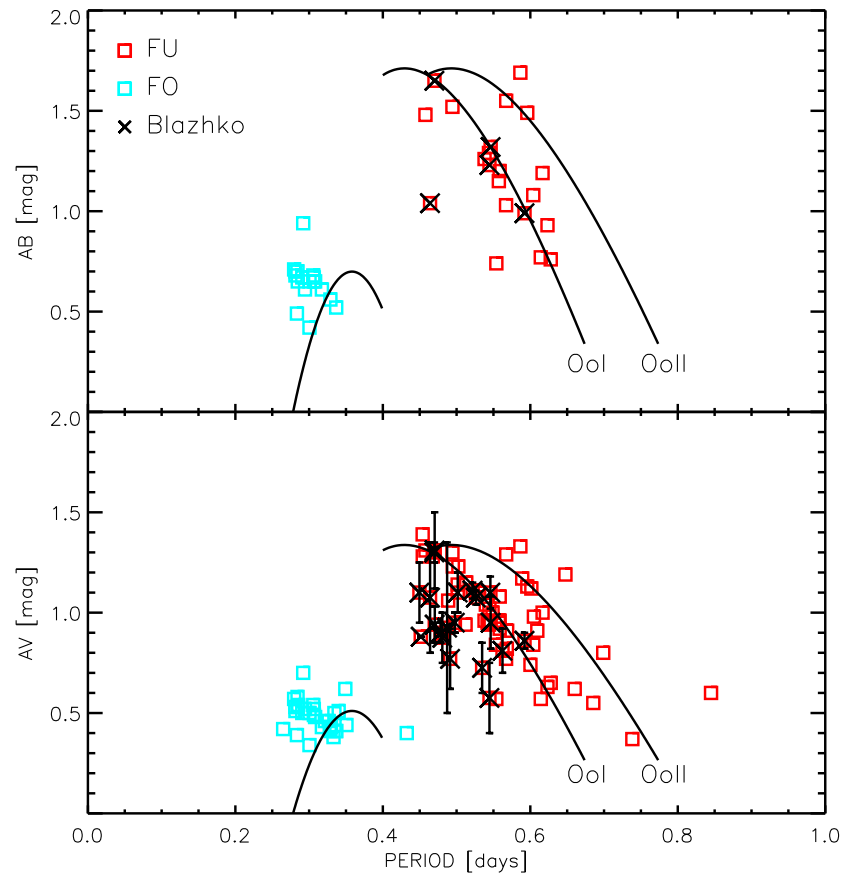


FIG. 16.— Same as Fig. 8, but for RR Lyrae stars in M5 (Szeidl et al. 2011). Top: B -band amplitude versus period. RR Lyraes pulsating in the fundamental and in the first overtone are plotted as red and cyan squares, respectively. Candidate Blazhko stars are marked with a black cross and the vertical bars display their range of brightness amplitude in the V band; the published data do not allow us to determine the range of brightness amplitude in B . Bottom: Same as the top, but for the V -band amplitude.

TABLE 1
LOG OF OBSERVATIONS IN OPTICAL BANDS.

Run ID	Dates	Telescope	Camera	<i>U</i>	<i>B</i>	<i>V</i>	<i>R</i>	<i>I</i>	Multiplex
1	pwm	1994 Apr 27	JKT 1.0m	EEV7	—	—	5	—	—
2	apr97	1997 Apr 14	ESO 0.9m	ccd\$33	—	—	8	—	8
3	bond5	1997 Jun 02	CTIO 0.9m	Tek2K ₃	6	5	5	—	5
4	manu	2000 Jun 07–09	ESO/Danish 1.5m	DFOSC Loral 2kx2k	1	146	5	—	—
5	wfi10	2000 Jul 08	MPI/ESO 2.2m	WFI	—	2	3	—	8
6	bond7	2001 Mar 28	CTIO 0.9m	Tek2K ₃	2	2	2	—	2
7	danish(a)	2001 Apr 14–18	Danish 1.5m	EEV 2kx4k	—	149	258	375	—
8	danish(b)	2001 Apr 27–May 05	Danish 1.5m	EEV 2kx4k	—	260	340	567	—
9	danish(c)	2001 May 08–13	Danish 1.5m	EEV 2kx4k	—	78	127	225	—
10	danish(d)	2001 May 25–30	Danish 1.5m	EEV 2kx4k	—	103	171	304	—
11	danish(e)	2001 Jun 24–Jul 01	Danish 1.5m	EEV 2kx4k	—	252	473	334	—
12	not017	2001 Jul 10	NOT 2.6m	CCD7	—	1	3	—	4
13	wfi6	2002 Feb 21	MPI/ESO 2.2m	WFI	—	4	4	—	4
14	wfi5	2002 Jun 18–21	MPI/ESO 2.2m	WFI	4	12	14	—	72
15	fors20602	2006 Feb 28	ESO VLT 8.0m	FORS2 MIT/LL mosaic	—	—	2	—	2
16	fors20605	2006 May 29–30	ESO VLT 8.0m	FORS2 MIT/LL mosaic	—	—	1	4	1
17	emmi8	2007 Jul 13–16	ESO NTT 3.6m	EMMI MIT/LL mosaic	—	19	19	11	15
18	Y1007	2010 Aug 03–04	CTIO 1.0m	Y4KCam ITL SN3671	—	84	84	—	—

NOTE. —

- 1 Observer: “PWM”
2 Observer: A. Rosenberg; data contributed by the observer
3 Observer: H. E. Bond; data contributed by the observer
4 Observer: unknown; data contributed by M. Zoccali
5 Observer: Ferraro; ESO program identification: 065.L-0463
6 Observer: H. E. Bond; data contributed by the observer
7 Observer: unknown
8 Observer: unknown
9 Observer: unknown
10 Observer: unknown
11 Observer: unknown
12 Observer: unknown (probably Bruntt?)
13 Observer: unknown; ESO program identification: 68.D-0265(A)
14 Observer: unknown; ESO program identification: 69.D-0582(A)
15 Observer: unknown; ESO program identification: 077.D-0775(B)
16 Observer: unknown; ESO program identification: 077.D-0775(A)
17 Observer: La-Silla-Sciops; ESO program identification: 59.A-9000
18 Observer: J.-W. Lee; SMARTS Project ID: Sejong10B

TABLE 2
LOG OF OBSERVATIONS IN NIR BANDS.

Run ID	Dates	Telescope	Camera	<i>J</i>	<i>H</i>	<i>K</i>	Multiplex	
1	m4ir	2002 Aug 16	ESO-NTT 3.5m	SOFI	50	—	50	—
2	mad3	2007 Jun 04–06	ESO VLT 8.0m	MAD	—	—	152	—
3	hawki11	2007 Aug 03–05	ESO VLT 8.0m	HAWKI	76	—	5	4
4	N10	2010 Sep 21	CTIO 4.0m	NEWFIRM	12	—	—	4
5	hawki3	2011 Mar 27	ESO VLT 8.0m	HAWKI	25	—	—	4
6	hawki4	2011 Apr 26	ESO VLT 8.0m	HAWKI	25	—	—	4
7	N1105	2011 May 19	CTIO 4.0m	NEWFIRM	26	13	24	4
8	hawki12	2011 Aug 23	ESO VLT 8.0m	HAWKI	45	—	—	4
9	hawki7	2012 May 16	ESO VLT 8.0m	HAWKI	20	5	22	4
10	hawki5	2012 May 17	ESO VLT 8.0m	HAWKI	16	—	21	4
11	hawki8	2012 Jun 21	ESO VLT 8.0m	HAWKI	62	12	21	4
12	hawki6	2012 Jun 22	ESO VLT 8.0m	HAWKI	—	16	21	4
13	hawki10	2012 Jun 27–28	ESO VLT 8.0m	HAWKI	53	43	42	4
14	hawki9	2012 Jul 14–15	ESO VLT 8.0m	HAWKI	16	20	26	4

Note. —

- 1 ESO Program ID 69.D-0604(A)
- 2 ESO Program ID Maintenance; PI-COI name Condor
- 3 ESO Program ID 60.A-9283(A)
- 4 NAO Proposal ID 2010A-0036; observers Probst, Zeballos
- 5 ESO Program ID 60.A-9800(L)
- 6 ESO Program ID 60.A-9800(L)
- 7 NAO Proposal ID 2011A-0644; observer Alonso-Garcia
- 8 ESO Program ID 60.A-9800(L)
- 9 ESO Program ID 089.D-0291(A)
- 10 ESO Program ID 089.D-0291(A)
- 11 ESO Program ID 089.D-0291(A), 60.A-9800(L)
- 12 ESO Program ID 089.D-0291(A)
- 13 ESO Program ID 089.D-0291(A)
- 14 ESO Program ID 089.D-0291(A)

TABLE 3
POSITIONS AND PERIODS FOR THE RR LYRAE VARIABLES IN M4.

ID	α (J2000.0)			δ (J2000.0)			Clement	Period ^a		T_0^b
	h	m	s	°	'	"		SL	LS	
V1	16	23	13.67	-26	30	53.6	0.2889	0.28888237	0.28888260	50601.4550
V2	16	23	16.30	-26	34	46.6	0.5357	0.53568190	0.53568192	50601.2750
V3	16	23	19.47	-26	39	57.0	0.5066	—	0.50667785	—
V5	16	23	21.03	-26	33	05.8	0.6224	0.62240130	0.62240109	50601.4778
V6	16	23	25.79	-26	26	16.3	0.3205	0.32051437	0.32051511	49469.6457
V7	16	23	25.95	-26	27	41.9	0.4988	0.49878480	0.49878722	50601.4511
V8	16	23	26.16	-26	29	41.6	0.5082	0.50822373	0.50822362	50601.6924
V9	16	23	26.80	-26	29	48.0	0.5719	0.57189461	0.57189448	50601.4580
V10	16	23	29.21	-26	28	54.3	0.4907	0.49071584	0.49071753	50601.2890
V11	16	23	29.98	-26	36	24.5	0.4931	0.49321080	0.49320868	52088.7604
V12	16	23	30.82	-26	34	58.9	0.4461	0.44610899	0.44610979	50601.5210
V14	16	23	31.29	-26	35	34.5	0.4635	0.46353167	0.46353112	50601.6818
V15	16	23	31.96	-26	24	18.1	0.4437	0.44371683	0.44366078	50601.6418
V16	16	23	32.50	-26	30	23.0	0.5425	0.54254940	0.54254826	50601.5688
V18	16	23	34.70	-26	31	04.6	0.4788	0.47879359	0.47879201	50601.5170
V19	16	23	35.05	-26	25	36.3	0.4678	0.46781097	0.46781107	50601.3741
V20	16	23	35.39	-26	32	35.9	0.3094	0.30941795	0.30941947	50601.6644
V21	16	23	35.93	-26	31	33.6	0.4720	0.47200727	0.47200741	50601.4735
V22	16	23	36.95	-26	30	13.0	0.6031	0.60306110	0.60306357	50601.4997
V23	16	23	37.33	-26	31	56.1	0.2986	0.29861522	0.29861557	50601.7160
V24	16	23	38.04	-26	30	41.8	0.5468	0.54678280	0.54678330	50601.3191
V25	16	23	39.42	-26	30	21.3	0.6127	0.61273466	0.61273480	50601.6449
V26	16	23	41.65	-26	32	41.1	0.5412	0.54121703	0.54121738	50552.3694
V27	16	23	43.17	-26	27	16.3	0.6120	0.61201625	0.61201831	50601.6926
V28	16	23	53.60	-26	30	05.3	0.5223	0.52234419	0.52234106	50552.6908
V29	16	23	58.25	-26	21	35.1	0.5225	0.51766400	0.52248466	46585.1061
V30	16	23	59.65	-26	32	34.3	0.2697	0.26974860	0.26974906	50601.7050
V31	16	24	00.64	-26	30	42.0	0.5052	0.50520360	0.50520423	50601.6277
V32	16	24	29.70	-26	32	02.5	0.5791	0.56578120	0.57910475	42890.5531
V33	16	24	33.33	-26	20	58.1	0.6148	0.61483030	0.61483542	43682.8820
V34	16	22	33.64	-26	24	46.6	0.5548	—	—	29723.338
V35	16	23	06.59	-26	30	27.0	0.6270	0.62702470	0.62702374	50601.4263
V36	16	23	19.45	-26	35	49.0	0.5413	0.54130500	0.54130918	50601.2199
V37	16	23	31.60	-26	31	30.6	0.2474	0.24736150	0.24734352	50601.5133
V38	16	23	32.87	-26	33	03.5	0.5778	0.57784690	0.57784632	50601.3413
V39	16	23	34.67	-26	32	52.1	0.6240	0.62395110	0.62395399	50601.4729
V40	16	23	36.49	-26	30	44.2	0.4015	0.38533000	0.38533005	50601.6088
V41	16	23	39.50	-26	33	59.8	0.2517	0.25174170	0.25174181	50601.5357
V42	16	24	02.00	-26	22	13.0	0.3037	0.30685490	0.31733120	46585.4073
V43 ^c	16	25	07.47	-26	25	43.9	0.3206	0.32066000	0.32068160	43681.1370
V49	16	23	45.25	-26	31	28.4	0.2160	0.22754460	0.22754331	50552.2894
V52	16	23	24.06	-26	30	27.8	0.4605	0.85549650	0.85549784	50601.0100
V61	16	23	29.76	-26	29	50.3	—	0.26528682	0.26528645	50601.5119
V64	16	23	15.06	-26	30	19.1	0.6033	0.60448250	0.60448407	50601.1695
V76	16	22	05.56	-26	21	43.1	0.3058	—	—	—
C1	16	23	36.43	-26	30	42.8	—	0.28625730	0.28625730	50601.4604
C2	16	24	07.59	-26	38	38.2	—	0.45480186	0.45480258	50601.6896

^a Pulsation periods (days) based on a compilation of literature values (Clement et al. 2001) or on our current data using either the string-length method (SL) or the Lomb–Scargle method (LS).

^b Epoch of maximum (HJD–2,400,000) estimated from the analytical fit of the V-band light curve, except V33 (T0 from Cacciari (1979)) and V34 from de Sitter (1947)

^c We have no data of our own for this star. The astrometry is based on measurements of three images from the Digitized Sky Survey, carefully transformed to our coordinate system. This is the position of a fairly isolated star of appropriate apparent brightness lying 0'.7 from the position given in Clement et al. (2001). The light-curve parameters are based on data from Cacciari (1979).

TABLE 4
MEAN OPTICAL MAGNITUDES AND AMPLITUDES FOR THE RR LYRAES IN M4.

ID	Period ^a days	U^b mag	B^b mag	V^b mag	R^b mag	I^b mag	A_U^c mag	A_B^c mag	A_V^c mag	A_R^c mag	A_I^c mag	Mode ^d
V1	0.28888260	14.56	14.02	13.43	13.00	12.54	0.44	0.57	0.44	0.36	0.24	RRc
V2	0.53568192	14.50	14.12	13.41	12.91	12.39	1.09	1.26	0.96	0.76	0.61	RRab*
V3	0.50667785	14.71	13.65	13.01	—	12.28	—	0.99	—	—	—	RRab
V5	0.62240109	14.57	14.12	13.37	12.84	12.28	—	0.43	0.33	0.26	0.20	RRab
V6	0.32051511	14.41	14.08	13.45	13.00	12.50	0.63	0.56	0.43	0.35	0.25	RRc
V7	0.49878722	14.56	14.09	13.42	12.94	12.40	—	1.39	1.06	0.86	0.70	RRab
V8	0.50822362	13.96	13.98	13.32	12.85	12.33	—	1.41	1.11	0.92	0.69	RRab
V9	0.57189448	14.48	13.98	13.30	12.82	12.30	—	1.44	1.11	0.91	0.71	RRab
V10	0.49071753	14.66	13.95	13.33	12.88	12.38	—	1.60	1.25	1.02	0.79	RRab
V11	0.49320868	14.53	14.07	13.40	12.93	12.41	0.92	1.24	1.07	0.86	0.65	RRab*
V12	0.44610979	14.49	14.23	13.58	13.10	12.54	1.60	1.61	1.28	1.06	0.81	RRab
V14	0.46353112	14.63	14.26	13.59	13.10	12.58	1.63	1.60	1.23	1.02	0.79	RRab*
V15	0.44366078	14.99	14.45	13.69	13.08	12.63	—	1.18	0.92	0.78	0.53	RRab*
V16	0.54254826	14.47	14.05	13.34	12.85	12.31	—	1.15	0.89	0.72	0.57	RRab
V18	0.47879201	14.66	14.02	13.36	12.88	12.35	—	1.45	1.12	0.92	0.71	RRab
V19	0.46781107	14.26	14.01	13.38	12.92	12.38	1.46	1.58	1.24	1.02	0.78	RRab
V20	0.30941947	14.27	13.72	13.19	12.80	12.33	—	0.36	0.23	0.22	0.14	RRc
V21	0.47200741	14.40	13.88	13.19	12.70	12.16	—	1.43	1.13	0.85	0.68	RRab
V22	0.60306357	14.60	14.08	13.33	12.81	12.24	—	0.66	0.48	0.40	0.30	RRab*
V23	0.29861557	14.28	13.75	13.19	12.78	12.41	—	0.56	0.43	0.35	0.27	RRc
V24	0.54678330	14.60	14.02	13.33	12.84	12.31	—	1.08	0.86	0.71	0.53	RRab*
V25	0.61273480	14.07	13.94	13.23	12.74	12.20	—	1.09	0.83	0.69	0.38	RRab
V26	0.54121738	14.46	13.87	13.25	12.79	12.27	—	1.57	1.24	1.01	0.78	RRab
V27	0.61201831	14.22	13.90	13.21	12.73	12.18	1.25	1.19	0.91	0.73	0.56	RRab
V28	0.52234106	14.07	13.79	13.19	12.75	12.23	1.16	1.27	1.01	0.78	0.90	RRab*
V29	0.52248466	14.20	13.90	13.28	12.83	12.31	1.10	1.40	1.08	0.96	0.79	RRab*
V30	0.26974906	14.16	13.84	13.32	12.94	12.48	0.58	0.66	0.51	0.40	0.32	RRc
V31	0.50520423	14.12	13.77	13.20	12.77	12.32	1.42	1.13	0.86	0.67	0.55	RRab*
V32	0.57910475	14.12	13.83	13.18	12.70	12.04	0.97	1.05	0.76	0.64	0.51	RRab
V33	0.61483542	13.94	13.65	13.03	12.58	12.08	1.23	1.21	0.95	—	0.59	RRab
V34	0.5548 ^e	15.47	14.73	14.02	—	12.77	—	—	—	—	—	RRab
V35	0.62702374	14.42	14.14	13.38	12.84	12.30	0.75	0.87	0.66	0.51	0.42	RRab*
V36	0.54130918	14.42	14.13	13.42	13.03	12.40	—	1.20	0.92	0.73	0.59	RRab
V37	0.24734352	14.45	13.90	13.37	12.99	12.51	—	0.28	0.22	0.18	0.14	RRc
V38	0.57784632	14.59	14.20	13.42	12.87	12.29	—	0.85	0.63	0.49	0.32	RRab*
V39	0.62395399	14.66	14.20	13.43	12.89	12.29	—	0.55	0.42	0.34	0.27	RRab*
V40	0.38533005	14.27	13.74	13.13	12.70	12.20	—	0.56	0.43	0.34	0.27	RRc
V41	0.25174181	14.61	14.03	13.49	13.09	12.64	—	0.45	0.36	0.28	0.25	RRc
V42	0.30685490	14.14	13.78	13.24	12.87	12.36	—	0.54	0.41	0.33	0.27	RRc
V43 ^f	0.32066000	13.86	13.60	13.08	—	—	0.52	0.58	0.43	—	—	RRc
V49	0.22754331	14.39	13.81	13.32	12.97	12.55	—	0.13	0.08	0.07	0.05	RRc
V52	0.85549784	14.28	13.90	13.11	12.56	11.97	0.41	0.39	0.31	0.25	0.19	RRab
V61	0.26528645	14.35	13.78	13.26	12.90	12.46	—	0.21	0.17	0.14	0.09	RRc
V64	0.60448407	21.42	20.74	20.01	19.50	18.93	—	1.08	0.84	0.68	0.54	RRab*
V76 ^e	0.3058	15.44	14.32	13.68	—	12.62	—	—	—	—	—	RR
C1	0.28625730	14.37	13.89	13.32	12.92	12.45	0.60	0.59	0.46	0.38	0.25	RRc
C2	0.45480258	17.46	16.71	16.04	15.83	15.07	—	1.63	1.23	—	0.77	RRab

^a Pulsation period based on the LS method.

^b Mean U, B, V, R, I magnitudes. The mean was computed as an intensity mean and then transformed into magnitude.

^c Luminosity amplitudes in U, B, V, R, I . The amplitudes were estimated as the difference between minimum and maximum of the analytical fit. The U amplitude is only available for a few variables (see Appendix).

^d Pulsation mode: RRab, fundamental; RRc, first overtone.

^e The period is the one given in the compilation of Clement. The tabulated magnitudes based on robust means of our data; we have insufficient data to fit a light curve.

^f Tabulated results based on published data from Cacciari (1979); the star lies outside our field.

TABLE 5
MEAN NIR MAGNITUDES AND AMPLITUDES FOR THE RR LYRAES IN M4.

ID	Period ^a days	J ^b mag	H ^b mag	K ^b mag	A _J ^c mag	A _H ^c mag	A _K ^c mag	Mode ^d
V1	0.28888260	11.79	11.50	11.42	0.12	0.09	0.08	RRc
V2	0.53568192	11.57	11.10	11.07	0.38	—	0.28	RRab*
V3	0.50667785	11.39	11.27	11.07	0.43	—	—	RRab
V5	0.62240109	11.40	11.17	10.94	0.19	—	—	RRab
V6	0.32051511	11.69	11.45	11.31	0.18	—	—	RRc
V7	0.49878722	11.59	11.16	11.14	—	—	—	RRab
V8	0.50822362	11.57	11.40	11.15	0.36	—	—	RRab
V9	0.57189448	11.45	11.02	10.96	0.54	—	—	RRab
V10	0.49071753	11.52	11.35	11.20	0.33	—	—	RRab
V11	0.49320868	11.64	11.22	11.22	0.36	—	—	RRab*
V12	0.44610979	11.73	11.36	11.25	0.48	—	—	RRab
V14	0.46353112	11.58	11.30	11.25	0.30	—	—	RRab*
V15	0.44366078	11.74	11.56	11.25	0.37	—	0.28	RRab*
V16	0.54254826	11.49	11.14	10.99	0.32	—	—	RRab
V18	0.47879201	11.63	11.40	11.08	0.42	—	—	RRab
V19	0.46781107	11.60	11.23	11.18	0.46	—	—	RRab
V20	0.30941947	11.58	11.41	11.26	0.18	—	—	RRc
V21	0.47200741	11.59	11.22	11.14	0.41	—	—	RRab
V22	0.60306357	11.38	11.03	10.89	0.31	—	—	RRab*
V23	0.29861557	11.65	11.40	11.29	0.08	—	—	RRc
V24	0.54678330	11.47	11.13	11.12	0.37	—	—	RRab*
V25	0.61273480	11.35	11.15	10.90	0.40	—	—	RRab
V26	0.54121738	11.51	11.24	11.02	0.46	—	—	RRab
V27	0.61201831	11.41	10.95	10.90	0.39	—	—	RRab
V28	0.52234106	11.53	11.15	11.07	0.52	—	—	RRab*
V29	0.52248466	11.44	11.16	11.04	0.31	—	—	RRab*
V30	0.26974906	11.82	11.59	11.48	0.16	—	—	RRc
V31	0.50520423	11.35	11.15	11.13	0.44	—	—	RRab*
V32	0.57910475	11.42	11.04	10.93	0.31	—	0.17	RRab
V33	0.61483542	11.35	10.92	10.88	0.41	—	0.29	RRab
V34	0.5548 ^e	11.50	11.21	11.06	—	—	—	RRab
V35	0.62702374	11.41	11.06	10.91	0.17	0.25	0.24	RRab*
V36	0.54130918	11.57	11.21	11.08	0.28	—	—	RRab
V37	0.24734352	11.84	11.69	11.51	0.06	0.07	—	RRc
V38	0.57784632	11.36	11.10	10.89	0.15	—	—	RRab*
V39	0.62395399	11.41	11.02	10.91	0.23	—	—	RRab*
V40	0.38533005	11.42	11.22	11.04	0.13	—	—	RRc
V41	0.25174181	11.90	11.66	11.58	0.14	—	—	RRc
V42	0.30685490	11.74	11.45	11.35	0.18	—	—	RRc
V43 ^f	0.32066000	—	—	—	—	—	—	RRc
V49	0.22754331	11.89	11.72	11.60	0.06	—	—	RRc
V52	0.85549784	11.06	10.68	10.60	0.13	—	—	RRab
V61	0.26528645	11.77	11.55	11.43	0.11	—	—	RRc
V64	0.60448407	18.05	—	17.40	0.16	—	—	RRab*
V76 ^e	0.3058	15.44	14.32	13.68	—	—	—	RR
C1	0.28625730	11.69	11.46	11.35	0.17	—	—	RRc
C2	0.45480258	14.28	13.76	13.72	0.2	—	—	RRab

^a Pulsation period based on the LS method.

^b Mean J,H,K magnitudes. The mean was computed as an intensity mean and then transformed into magnitude.

^c Luminosity amplitudes in J,H,K. The amplitudes were estimated as the difference between minimum and maximum of the analytical fit.

^d Pulsation mode: RR_{ab} , fundamental; RR_c , first overtone. An asterisk marks the variables that are candidate Blazhko variables.

^e The period is the one given in the compilation of Clement. The tabulated magnitudes based on robust means of our data; we have insufficient data to fit a light curve.

^f Outside our field of view.

TABLE 6
POSITIONS AND MEAN OPTICAL PHOTOMETRY FOR OTHER CANDIDATE VARIABLE STARS.

ID	α (J2000.0)			δ (J2000.0)			U	B	V	R	I	period (d) or comment
	h	m	s	°	'	"						
V53	16	23	14.43	-26	36	05.4	14.64	12.73	10.88	9.80	9.04	variable?
V54	16	23	42.82	-26	29	27.5	17.79	13.98	12.66	11.86	11.06	LPV or EB?
V55	16	23	45.93	-26	23	36.9	14.22	13.70	13.24	—	12.59	LPV or EB?
V56	16	23	45.95	-26	33	38.8	15.02	14.24	12.93	12.13	11.35	LPV or EB?
V57	16	23	21.17	-26	31	59.7	14.58	14.12	12.99	12.28	11.56	LPV or EB?
V58	16	23	47.84	-26	32	05.9	14.30	13.83	13.50	13.24	12.94	LPV or EB?
V59	16	23	50.15	-26	33	23.8	14.66	14.35	13.44	12.81	12.17	LPV or EB?
V60	16	23	45.23	-26	33	56.8	15.54	14.82	13.56	12.79	12.02	LPV or EB?
V63=K44	16	23	21.05	-26	33	25.0	18.97	18.82	17.80	17.14	16.49	0.26358410
V65=K46	16	23	47.19	-26	31	56.5	18.85	18.85	18.58	18.39	18.16	LPV or EB?
V66=K47	16	23	25.57	-26	29	11.7	17.98	17.77	16.93	16.37	15.77	0.26987521
V67=K48	16	23	36.81	-26	31	44.1	17.27	17.12	16.25	15.65	15.09	0.28269412
V68=K49	16	23	34.35	-26	32	01.8	19.32	18.26	17.03	16.26	15.49	0.29744408
V69=K50	16	23	31.34	-26	31	48.4	18.27	18.18	17.32	16.74	16.21	0.26600006
V70=K51	16	23	33.22	-26	31	09.1	17.92	17.89	17.00	16.40	15.83	0.30368223
V71=K52	16	23	31.50	-26	30	57.7	17.84	17.67	16.70	16.03	15.39	0.776468
V72=K53	16	23	38.51	-26	32	10.8	16.76	16.46	15.83	15.40	15.01	0.30844869
V73=K54	16	23	50.96	-26	34	42.1	18.90	18.72	17.78	17.14	16.54	0.25246449
V74=K55	16	23	45.78	-26	31	16.5	17.64	17.70	16.87	16.31	15.72	0.31070264
V75	16	22	51.68	-26	25	14.7	14.50	14.31	13.37	—	12.14	insufficient data
V77=K56	16	23	34.30	-26	29	55.9	16.32	15.83	14.66	13.92	23.21	possible EB
V78=K57	16	23	36.73	-26	31	50.6	16.57	16.24	15.20	14.53	13.86	not variable?
V79	16	24	01.20	-26	21	56.2	16.74	16.18	15.07	—	13.69	insufficient data
V80	16	23	48.94	-26	23	51.9	17.05	16.66	15.60	—	14.25	not variable?
K59	16	23	39.18	-26	29	54.8	—	21.69	20.27	19.27	18.40	0.7114224
K60	16	23	47.50	-26	32	12.6	17.75	17.62	16.77	16.19	15.60	0.3703839
K61	16	23	42.35	-26	33	17.9	16.60	16.29	15.70	15.29	14.83	not variable?
K62	16	23	32.62	-26	36	13.1	20.05	19.74	19.13	18.72	18.22	0.04088083
K63	16	23	27.37	-26	32	26.6	16.80	17.78	17.67	17.55	17.42	LPV or EB?
K64	16	23	20.80	-26	31	02.2	19.43	19.07	18.44	18.02	17.55	not variable?
K65	16	23	28.41	-26	30	21.8	17.57	17.44	16.52	15.90	15.27	2.293172
K66	16	23	32.26	-26	31	41.1	17.71	17.64	16.78	16.20	15.64	8.11289
K68	16	23	38.59	-26	30	30.9	16.14	15.84	15.24	14.82	14.38	not variable?
K69	16	23	58.11	-26	37	18.9	17.93	17.89	17.01	16.43	15.81	48.195 ^a
C3	16	23	35.59	-26	27	08.1	18.53	18.01	16.80	16.01	15.24	19.4651
C4	16	23	44.79	-26	24	29.3	16.30	16.08	15.17	14.58	13.98	0.4385898
C5	16	23	34.60	-26	25	41.4	20.39	19.82	19.00	18.45	18.02	0.41970602
C6	16	23	59.77	-26	29	43.6	19.32	19.12	18.06	17.37	16.72	0.26297749
C7	16	24	02.14	-26	30	51.9	21.32	20.15	18.90	18.13	17.28	0.27161155

^a Because of the haphazard cadence of our observations, this star is subject to extreme aliasing problems. Left to ourselves, we would not have been able to determine a secure period. Kaluzny et al. (2013a) give the period of this star as 48.19 d, and this is the best period we were able to find between 48.1 and 48.3 d. Many other periods outside this range would be possible if our data were all that were available.

TABLE 7
MEAN INFRARED PHOTOMETRY FOR OTHER CANDIDATE VARIABLE
STARS.

ID	<i>J</i>	<i>H</i>	<i>K</i>	comment
V53	11.14	9.40	9.28	probably saturated
V54	9.82	9.29	8.96	probably saturated
V55	12.06	11.91	11.79	
V56	10.11	9.62	9.32	probably saturated
V57	10.44	10.18	9.90	probably saturated
V58	12.46	12.38	12.28	
V59	11.21	10.80	10.62	possibly saturated
V60	10.80	10.37	9.98	probably saturated
V63=K44	15.55	14.81	14.69	
V65=K46	17.82	17.44	17.06	
V66=K47	14.92	14.43	14.34	
V67=K48	14.74	14.50	14.47	
V68=K49	14.49	13.89	13.69	
V69=K50	15.38	14.98	14.58	
V70=K51	15.05	14.58	14.33	
V71=K52	14.57	13.99	13.79	
V72=K53	14.29	14.13	13.90	
V73=K54	15.57	14.98	14.75	
V74=K55	14.80	14.48	14.26	
V75	11.31	10.85	10.82	possibly saturated
V77=K56	12.05	11.38	11.20	
V78=K57	12.78	12.22	12.06	
V79	12.68	12.08	11.87	
V80	13.25	12.63	12.48	
K58	15.00	14.52	14.37	
K59	16.97	16.00	15.82	
K60	16.72	16.20	15.95	
K61	14.11	13.92	13.81	
K62	17.46	17.39	17.14	
K63	17.17	17.74	17.24	
K64	16.86	16.45	16.32	
K65	14.47	13.88	13.79	
K66	14.73	14.36	14.13	
K68	13.67	13.44	13.29	
K69	14.92	14.46	14.35	
C3	14.04	13.41	13.11	
C4	13.15	12.71	12.55	
C5	16.98	16.62	16.64	
C6	15.71	15.08	14.82	
C7	16.26	15.48	15.27	